BEAM CHARACTERISTICS OF CONTACT CONES FOR USE IN ENDOCAVITARY IRRADIATION

A Thesis

Submitted to the Graduate Faculty of the
Louisiana State University and
Agricultural and Mechanical College
in partial fulfillment of the
requirements for the degree of
Master of Science

in

Nuclear Science
(Medical Radiation Science Option)

by
William Tyrone Fontenot
B.S., Tulane University, 1983
May 1985

Dedicated to

My Parents,

Bill and Starr Fontenot

ACKNOWLEDGEMENTS

I would like to express my thanks to William S. Kubricht for his time and advice. I would also like to thank Dr. Sheldon A. Johnson for his much needed advice.

I would like to express my appreciation to Dr. Edward N.Lambremont and Dr. Ronald M. Knaus for their advice and encouragement.

A special note of appreciation to Dr. Robert Shalek for taking time out of his schedule to serve on my exam committee.

Words cannot describe my appreciation for the sacrifice made for me and the support given to me by my wife, Gigi, during this period of our life.

TABLE OF CONTENTS

LIST OF TABLES

LIST OF FIGURES

LIST OF ABBREVIATIONS

kVp	kilovolt potential
MeV	million electron volts
MV	million volts
rad	radiation absorbed dose
TSD	target to surface distance

ABSTRACT

The uses of contact cones in cancer radiotherapy are continuing to expand in a variety of ways. They are being used transorally, transrectally, transvaginally, and in the abdominal region during surgery. Due to the fact that contact cones are usually of unique design and construction, published data on existing cones should not be used for dose calculations with other cones. The purpose of this thesis is to determine the clinically significant beam characteristics of the contact cone and accessory systems at the Perkins Radiation Treatment Center located in Baton Rouge, Louisiana. Optimal collimator setting, percent depth dose, and isodose curves were determined empirically. Also, the electron beam energy at the surface of a phantom, range of the electrons, percent photon contamination, and dose calibration factors were determined from this study. Although the dose calibration factors presented herein for contact cones are the most important results of this work, the remaining data should improve a physician's technical capability for treating cancer by electron therapy.

INTRODUCTION

External beam irradiation is the most frequently used radiation technique in treating cancer. The success of external beam irradiation is partially due to the variety of methods by which the beam may be modified. A contact cone is an important accessory for shaping or restricting external radiation beams, and has been in use since the early 1930's. Contact cones consist of an inner sleeve normally lucite, that maintains the structural integrity of the cone, and an outer sleeve often made of soft lead to restrict scattering of the radiation beam (Figure 1). Contact cones can vary in diameter, length, degree of bevel, and construction materials. The design of a contact cone often is dependent upon the anatomical site in which it is to be used.

Contact cones are used in the treatment of cancer because of their ability to remove healthy tissue from the path of the beam of radiation, to acquire high positioning reproducibility, and to visualize directly the treatment area. For most clinical purposes, contact cones are used with either a primary treatment or with boost treatments combined with conventional external beam irradiation. In the primary modality, the contact cone is used during all or most of the treatment. In boost technique, the contact cone is present during only a portion of the treatment and is removed for later

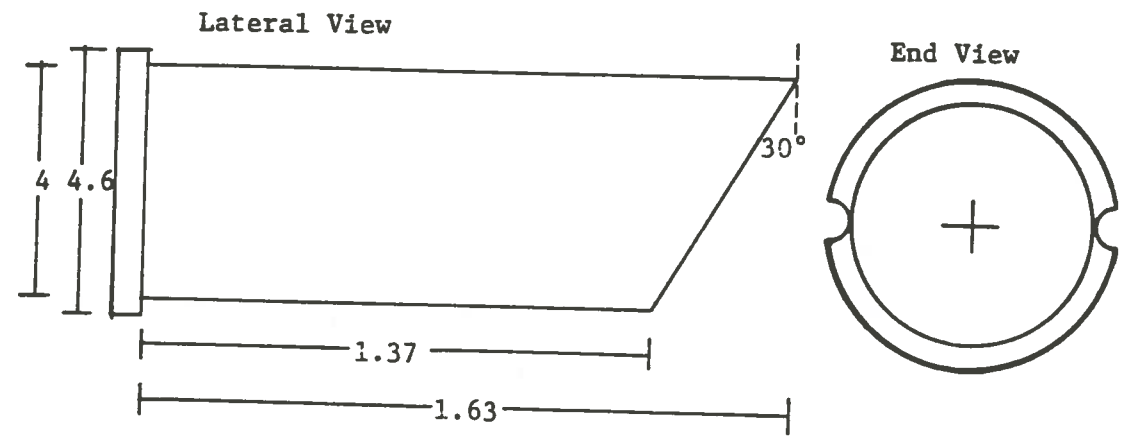

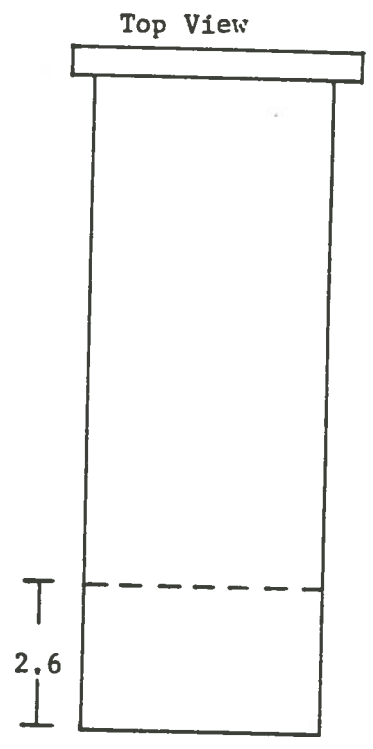

Figure 1. Sketch of a typical 4.0 cm contact cone as used at Perkins Radiation Center. All Measurments in cm.

external beam irradiation of a larger volume. Due to the versatility of contact cones they are being used to treat cancers in oral, rectal, thoracic, and abdominal regions of the body.

Although contact cones had been used in earlier treatment regimens the first major work was done in the mid 1940's by Del Regato (1948). He worked with transvaginal cones using 140 kVp x-rays for the treatment of carcinoma of the cervix. Del Regato (1952) pioneered most of the early work in transvaginal cone irradiation, using it as a boost technique. Later, transvaginal cone irradiation as a boost and a primary modality was becoming a common method of treatment (Nolan 1960, Scaramucci 1958). By the mid 1950's, as reported by Wang (1980), selected lesions in the oral cavity were being treated as a boost technique using 280 kVp x-rays and contact cones. By the 1970's, contact cones used with orthovoltage (150-200 kVp) x-rays were a common form of cancer treatment (Fagos 1967, Griffin 1977, Phillips 1968).

Between the mid 1960's and the mid 1970's, contact cones were beginning to be used with electron beams. The electron beam offered several significant improvements compared with an orthovoltage x-ray beam. The major improvements were the unique characteristics of the electron beam, such as the shallow depth of maximum dose and the sharp falloff of the depth dose curve (Figure 2).

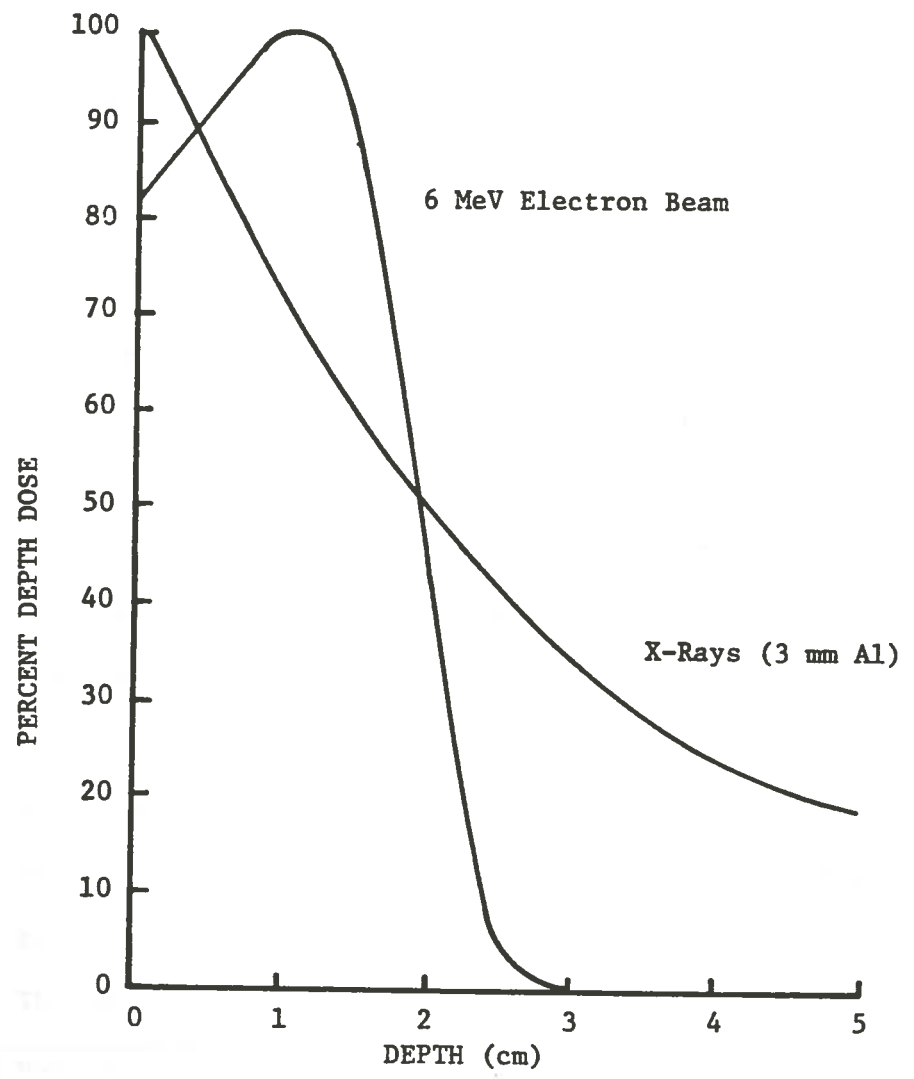

Figure 2. Comparison of percent dose curves for a 6 MeV electron beam and low energy x-ray beam. It is noted that a depth of 3 cm the dose delivered by the electron beam is essentially zero, whereas the dose delivered by the 125 kVp x-ray still retains approximately 37% of the maximum dose.[White 1983]

Also orthovoltage machines were becoming obsolete and were only being used for special cases (such as contact cone therapy). In the conversion from orthovoltage to electron beams, the connecting apparatus between the machine's head and the contact cone (called the applicator) needed to be modified for contact cone therapy.

Rich (1984) has reported that contact cones were being experimented with in surgery as far back as the early 1900's, but it was not until the early 1970's that intraoperative radiation was being applied on a large scale in the treatment of cancer (Abe 1981, Abe 1975, Fairchild 1947, Rich 1984). Intraoperative radiation has been used to treat subcutaneous skin lesions (Watson 1943), in the head and neck area (Rich 1984), and in the thoracic region. In the last ten to fifteen years, considerable work has been done in the abdominal area. Intraoperative therapy has advanced rapidly in recent years and many new cancer sites such as abdominal lymph nodes and pancreatic cancers may now be treated (Wood 1981, Hirdake 1975). The intraoperative contact cone is a useful tool when the cone is used as a boost, primary, or palliative technique in surgery (Metzger 1983, Abe 1981).

Many new designs and modifications of contact cones are being developed. For example, contact cones are now being modified to include a lighted mirror system to allow the physician to observe

directly the treatment area thus enhancing reproducibility (Swindell 1983, Wilenzick 1983). Another modification is a safety break-away cone (Figure 3), which allows the cone to break-off when too much pressure is applied.

Contact cones are quite frequently used in short treatment regimens. For example, a cone may be used for one treatment with intraoperative therapy or two or three treatments with endocavitary radiation. These short treatment regimens can result in high doses (600-2000 rad) delivered in one treatment. Because of such high doses, a small fluctuation in the output of the beam due to a change in the contact cone system could cause a significant difference in the dose delivered.

The differences in contact cone systems can be related to a number of factors; the therapy machines design, the type of radiation (electrons or x-ray), shape and size of the contact cones, materials used in its construction, and the design of the applilcator. Therefore, dose calibrations must be made for each and every individual system, and one cannot rely on published data from other systems. Furthermore, the data should be taken empirically for each individual cone and for each energy at energy at which it will be used.

The purpose of this thesis is to determine and analyze the

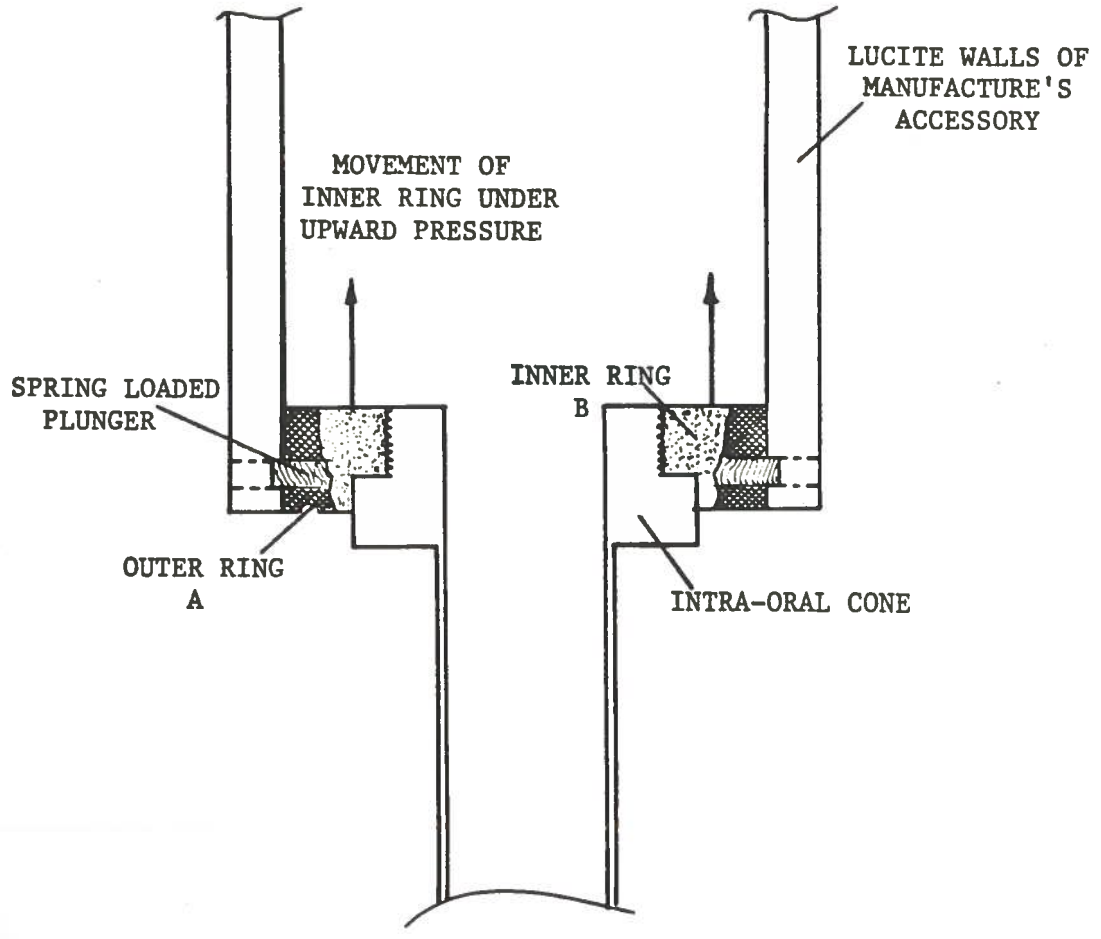

Figure 3. Drawing of a break-away safety contact cone.[Briggs 1984]

clinically significant beam characteristics for the contact cone system used at the Perkins Radiation Treatment Center.

MATERIALS AND METHODS

All measurements in this thesis were made with a Varian Clinac 18, an 18 MeV standing wave radio-frequency powered linear accelerator. The Clinac 18 is capable of producing 10 MV photons and 6, 9, 12, 15, and 18 MeV electron beams at an average dose rate of 300 rad/min.

The contact cone system used at Perkins Radiation Treatment Center is a unique design. The four contact cones consist of an inner lucite sleeve and an outer lead sleeve approximately 1 mm thick. A lucite obturator facilitates the intravaginal insertion of the cone. The four contact cones in use at Perkins Radiation Treatment Center have diameters of 2.5, 3.0, 3.5, and a 4.0 cm. All the cones have a 30 degree beveled end. Perkins Radiation Treatment Center's principal use of the contact cone is cervical cancer and the beveled end allows a good contact with the cervix.

The contact cone applicator, which is the fitting that connects the contact cone to the head of the Clinic 18, has a built-in luminating mirror system. This mirror allows the treatment area to be observed directly. The contact cone can be rotated 360 degrees on its own axis.

In this thesis, field flatness, depth dose curves, isodose curves,

photon contamination, energy of the beam, and calibration factors of the four contact cones were measured. Two methods of dosimetry were used. Film dosimetry was employed to find the field flatness and the beam profiles (isodensity curves, which when modified give isodose curves). Ion chamber dosimetry was used to measure the relative ionization data from which depth dose curves, photon contamination, energy, and calibration of the contact cones were derived.

Film dosimetry is an excellent practical method for high energy electron dosimetry, if potential variables are held to a minimum (Tapley 1976). For purposes of dosimetry, film was placed in a masonite tissue-equivalent phantom (30x55x38 cm). Care was taken to place the film into the phantom, so that the film did not extend over or under the edge of the phantom. Additionally, the air gap in the film's packet must be removed. In this study, the air was removed by placing pinholes in the film packet and allowing the pressure of the phantom closing to force the air out. Failure to assure proper alignment of the film and to remove the air gaps could cause incorrect readings (Figure 4).

An important consideration in the determination of the quality of film dosimetry is linearity. If all data are taken in the linear density range of the film, then small variations in dose will correlate

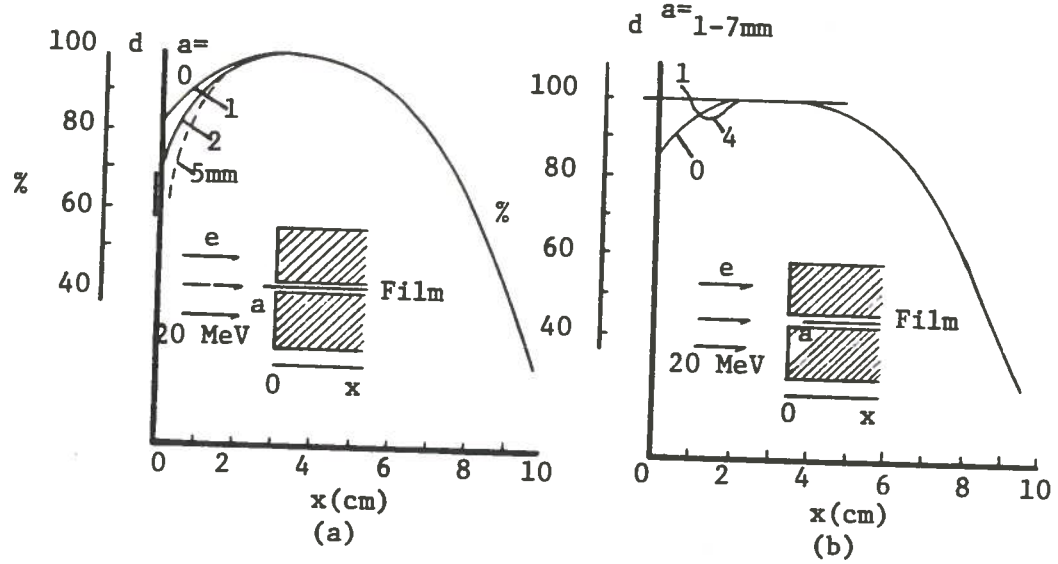

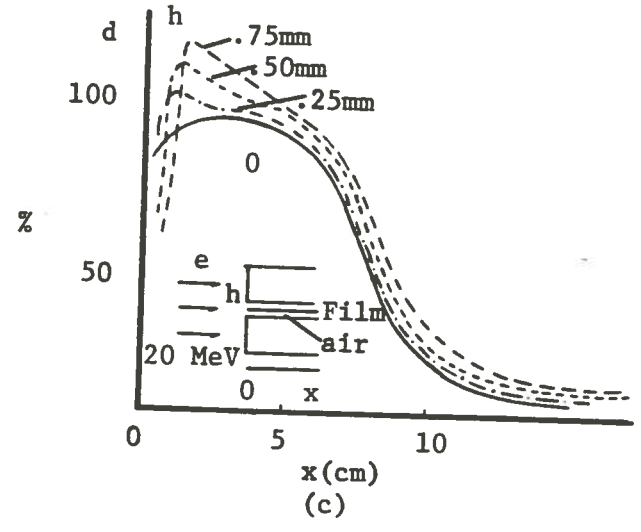

Figure 4. Influence on the depth density curves of misalignment of the film in the phantom. Three effects can be observed: (a) if the film extends beyond the phantom, (b) if it is recessed within the phantom, and if (c) there are any gaps between the film and the phantom.[Tapley 1976]

directly to small variations in density. Film linearity was determined with 6 MeV and 9 MeV electron beams. Kodak X-Omatic V film, Ready Pack XV-2 (25x30 cm) was used throughout this study. All exposed film was developed by a Kodak PR X-Omat Processor, which is automatic and rapid. Each film was divided into four equal quadrants, and each quadrant was then exposed to a single dose using a 4x4 cm electron beam cone. Doses were increased in regular increments. Lucite material (Figure 5) was placed on top of the film to assure the proper build-up of electrons which produce the dose. The density of each quadrant of the developed film was read with a MacBeth TD504 manual densitometer. A film variance test was done to determine the variation between individual films. A machine setting of 200 monitor units was given to each film with a 6 MeV electron beam using a 4x4 cm electron cone. The film was developed and read (MacBeth densitometer) to determine the amount of variance among the films.

The optimal collimator setting at which to operate the contact cones at each energy was ascertained with film dosimetry. In the determination of the collimator setting, the film and the masonite phantom were used (Figure 6). With the film parallel to the beam, the first trial was done with the 6 MeV electron beam and the 2.5 cm cone. Exposures of 200 monitor units were made at collimator settings of 15x15, 12x12, 10x10, 8x8, 6x6, and 4x4 cm. The exposed film was developed and then placed in the Artronic Isodenstiometer

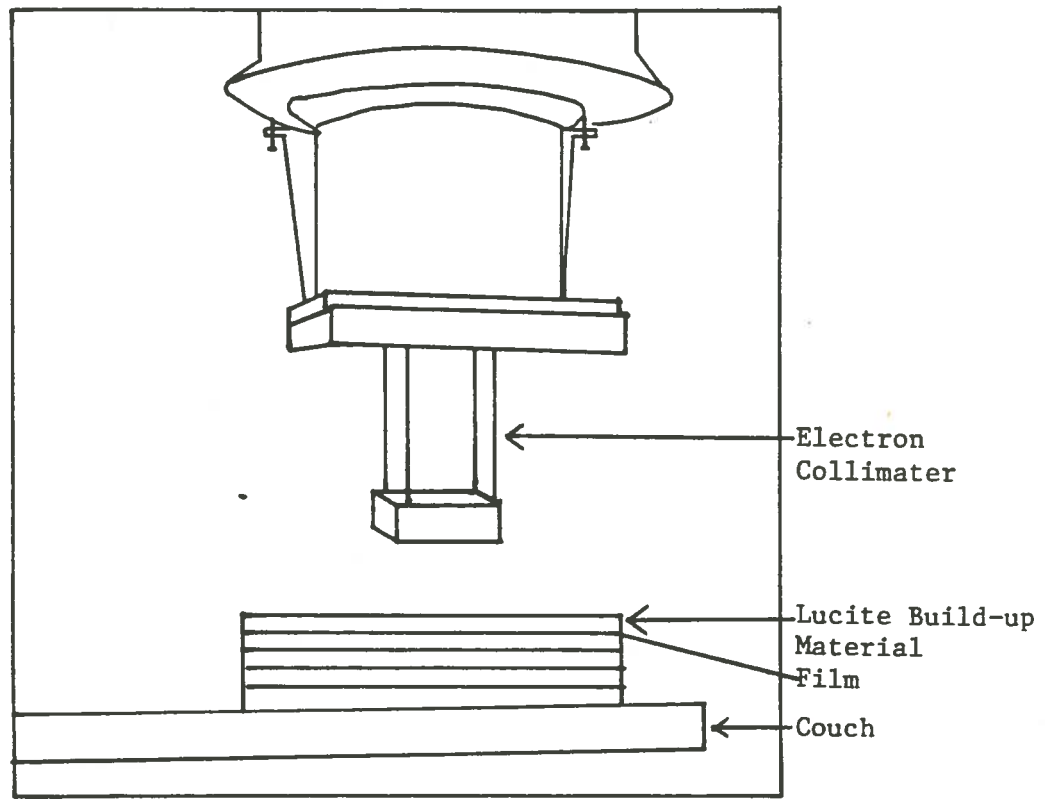

Figure 5. Film linearity test arrangement. 4x4 cm electron collimator setting at 100 TSD.

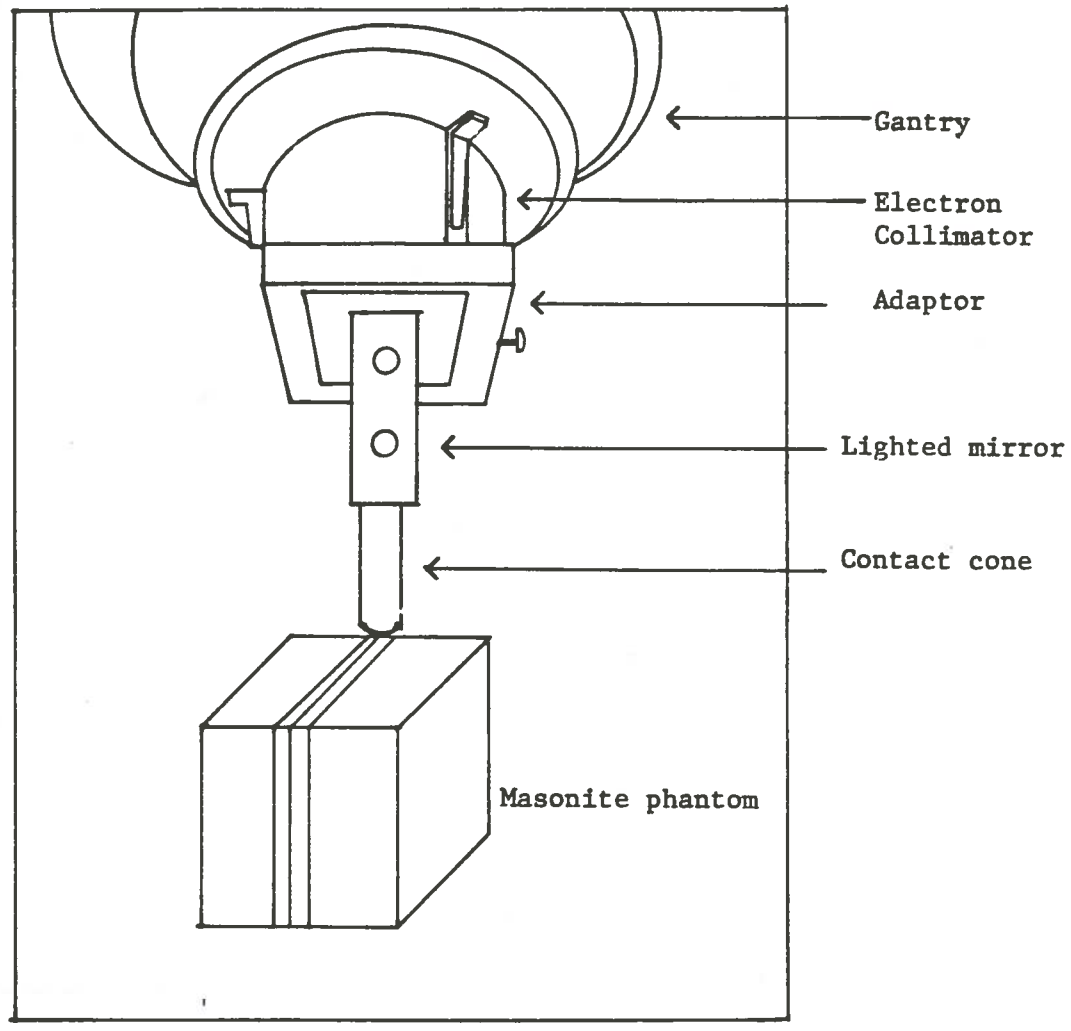

Figure 6. Collimator setting arrangement. Contact cone brought in contact with masonite phantom. Not shown is the clamping device that holds the phantom together.

Model 1705 automatic density reader. The densitometer produced beam profile (field flatness) curves for each of the collimator settings. From this trial it was determined that a 12x12, 8x8, and 4x4 cm could be eliminated due to their similarity to a 15x15, 10x10, and 6x6 cm setting. Therefore, a 15x15, 10x10, and 6x6 cm collimator setting were used at all the energies for each cone size. These films were developed and analyzed by the densitometer. Densitometer readings were analyzed to determine the optimal collimator setting for each cone at each energy.

The isodensity data were obtained from the films of the 10x10 cm collimator settings for each cone at each energy. The developed film was placed into the Artronic densitometer in auto mode. The densitometer produced a complete set of isodensity curvese for each film ranging from 20 to 90%.

Relative ionization data were obtained by ion chamber dosimetry. The ion chamber used was a 0.1 cc PTW Model #31-301 with an internal radius at 1.9 mm, which was connected by a shielded triax cable to a Keithly 615 Digital Electrometer with a 300 volt DC external power supply. The ion chamber was mounted through a plastic goose-neck in a 28x28 cm lucite water phantom as seen in Figure 7. The phantom was modified to accomodate the 30 degree bevel on the end of the contact cones. The ion-chamber probe lowering mechanism was re-aligned at a 30 degree angle to the base of the phantom. This allowed the

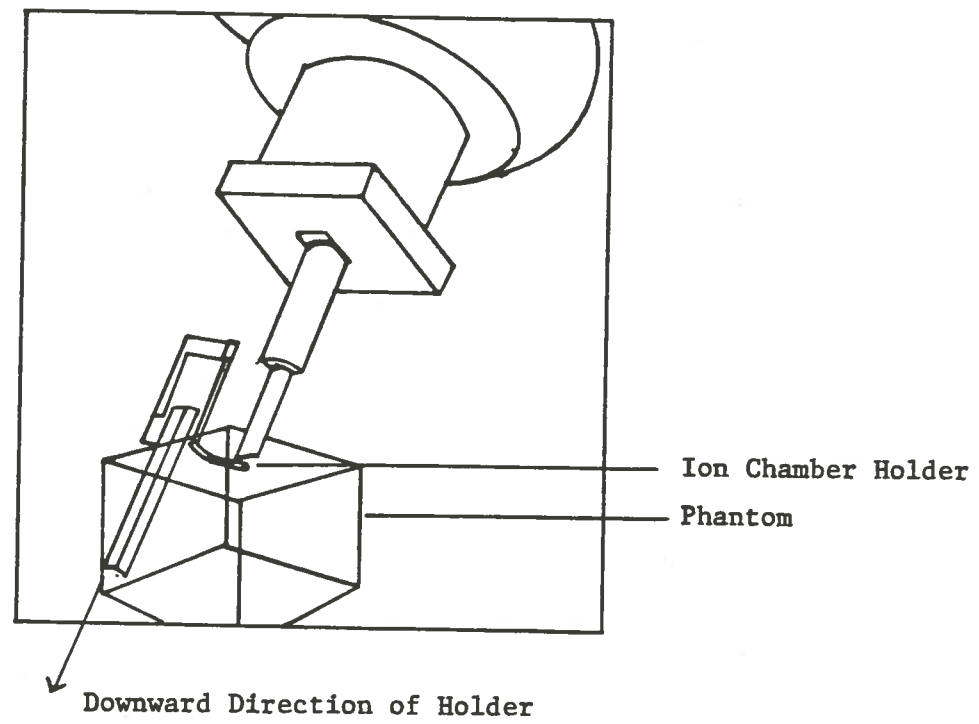

Figure 7. Arrangement of ion chamber and water phantom to measure relative ionization.

ion-chamber to be raised or lower along the central axis of the beam after the gantry was angled 30 degrees off the vertical. With the gantry angled, the contact cone could be brought to a parallel contact with the surface of the water in the phantom. The ion-chamber was raised as close to the contact cone as possible and then centered on the beam's crosshairs. With the 6 MeV electron beam and the 2.5 cm contact cone, a polarity test was run. Positive and negative polarity data was obtained as varying depths. Less than 1% variation was found between the positive and negative readings. Therefore, the remainder of the relative ionization data were obtained with negative polarity.

The range of electrons (Rp), the energy of the beam (Eo), and the photon contamination were determined from the relative ionization data. The electron range is defined as the depth at which extrapolation of the straight descending part of the curve meets the extrapolation line of the background due to x-rays (See point Rp on Figure 8). The extrapolated background line is commonly called the "tail".

The percent photon contamination of the depth dose curve is determined from the tail. The dose percentage of the tail is referred to as the percent photon contamination.

The energy of the electron beam is an important concept. The

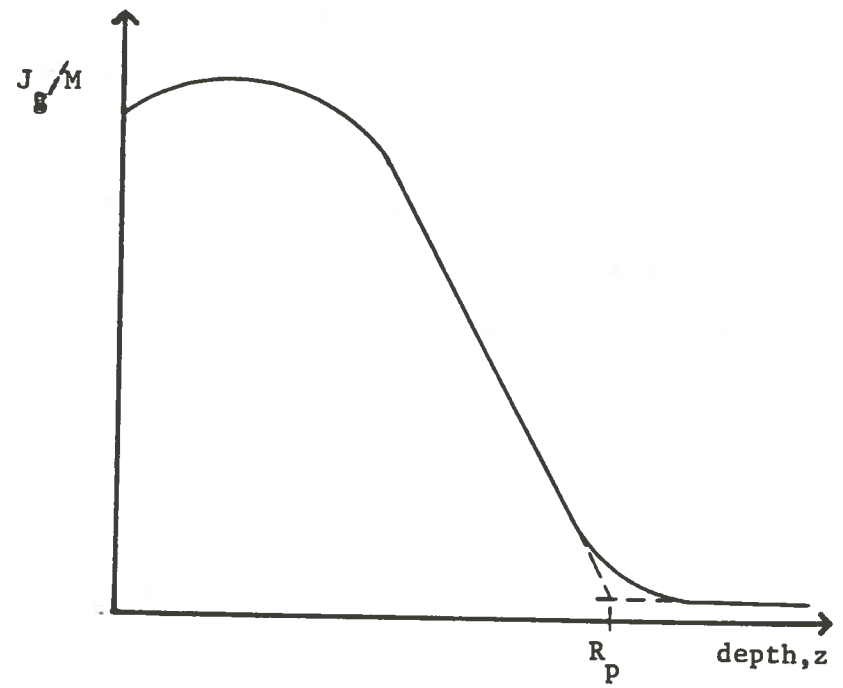

Figure 8. Definition of the practical range of electrons. Drawn is the measured value of J_g, relative to an arbitrary monitor value, M, as a function of depth, z, in the absorber. [ICRU 1976]

energy of the electron beam cannot be characterized by a single parameter. The energy of the electron beam can be defined as the accelerator energy (Ea), the energy at surface (Eo), or the energy at a point in the phantom or medium (Ez) as represented in Figure 9. The accelerator energy (Ea) is defined as the energy at a point on the inner side of the accelerator window. The energy distribution at this point usually plots as a very narrow peak, which can be characterized by a single energy. After the electron beam has passed through the exit windows, scattering foils, mirrors, monitor chambers, and air column the electron beam has substained energy losses. These energy losses shift the spectrum to lower energies and broaden the spectrum. The modified energy at the surface of the phantom is defined as energy at the surface (Eo). After the electron enters the phantom, the calculation of energy (Ez) becomes very difficult. In the phantom, the energy losses can amount to the total energy of the beam if the depth of the phantom is beyond the range of the electrons. The energy of the beam at the surface was determined from the range of the electrons by the formula (ICRU, 1971);

$$Eo=0.722 + 1.92xRp$$

Eo represents the energy of the beam at the surface of the phantom.

To determine the dose being delivered at depth to the water phantom by the contact cones a calibration factor needed to be determined for the PTW ion chamber. A calibration comparison was

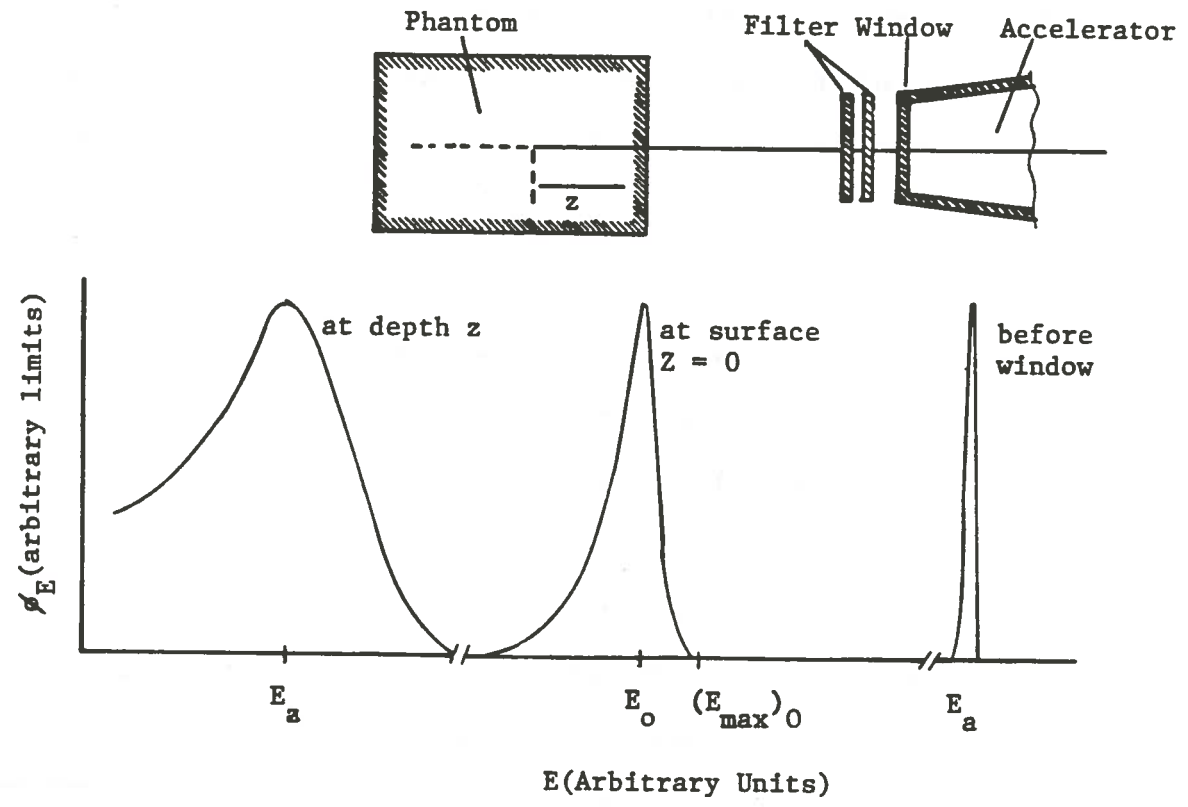

Figure 9. Representation of the possible energy spectra that can be defined for an accelerator beam.

made with the PTW ion chamber and a Farmer 0.2 cc ion chamber Model 2505/3. The PTW chamber was placed in a lucite 25x25 water phantom at a depth of 1.0 cm. An exposure of 173.7 rad was delivered with the Cobalt-60 machine to the chamber. The Farmer ion chamber was placed in the exact arrangement as the PTW ion chamber and given 173.7 rad. The calibrated Farmer ion chamber data were then compared to the PTW ion chamber data to obtain the chamber factor. The dose to a given depth in the water was determined by the formula;

$$Dw = R \times N \times Ce \times Ct \times Cp$$

where DW = dose in water
R = reading on electrometer
N = chamber factor
Ce = roentgen to rad conversion factor
Ct = temperature correction
Cp = pressure correction

The roentgen to rad conversion factor (Ce) is dependent upon the energy of the beam and the depth in the phantom. The Ce was calculated from the relative ionization data by the formula;

$$Ce = 0.97 \times Ez\ ((exp)-.048)$$

The perturbation factor of less than 1% was ignored in this study. The dose delivered at a given depth in the water was then divided by the number of monitor units delivered to calculate the number of rad delivered per monitor unit.

RESULTS

When film is used for dosimetry with high energy electrons, the film's reliability must be determined. Figure 10 represents the film linearity test determined with 6 MeV and 9 MeV electrons. The exposures to the films ranged from 100 to 400 rad in 50 rad increments. The optical density of the developed film was plotted as a function of absorbed dose. From the data in Figure 10, the linear regions for both curves were found to be in the 150 to 200 rad range. A setting of 200 monitor units was chosen because this allowed for minimum exposure times necessary to achieve results. Furthermore, 200 monitor units allowed us to work in the linear region, thus would result in small variations in the dose relating to small variations in the optical density of the film. Tests of film to film variance gave identical optical density readings of 1.06. Therefore, when comparing one developed film to another of the same type, an error of less than 0.1% should be expected. This assumes that background has been taken into account.

The initial test for the optimal collimator setting was conducted with 6 MeV electrons and the 2.5 cm contact cone. Beam profiles (field flatness) were plotted for collimator settings of 15x15, 12x12, 10x10, 8x8, 6x6, and 4x4 cm. As seen in Figure 11, the beam profiles were plotted relative to the maximum density of the 15x15 cm film.

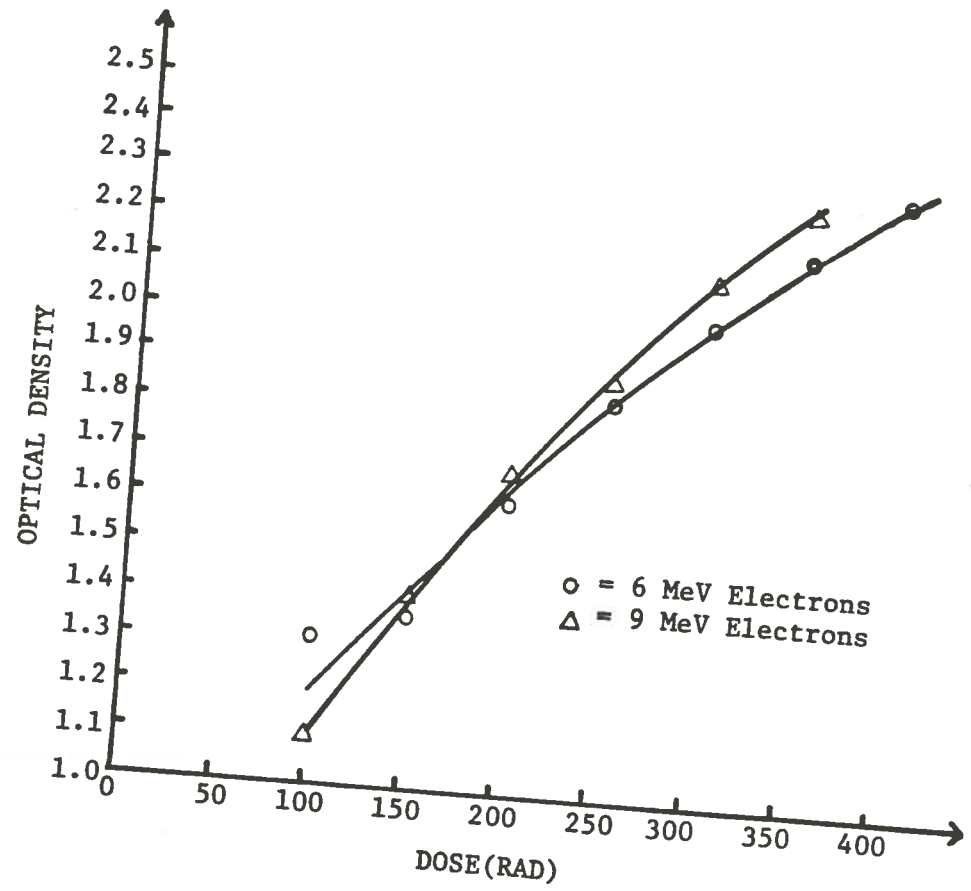

Figure 10. Results of film linearity test. Net optical density (density minus background) verses absorbed dose.

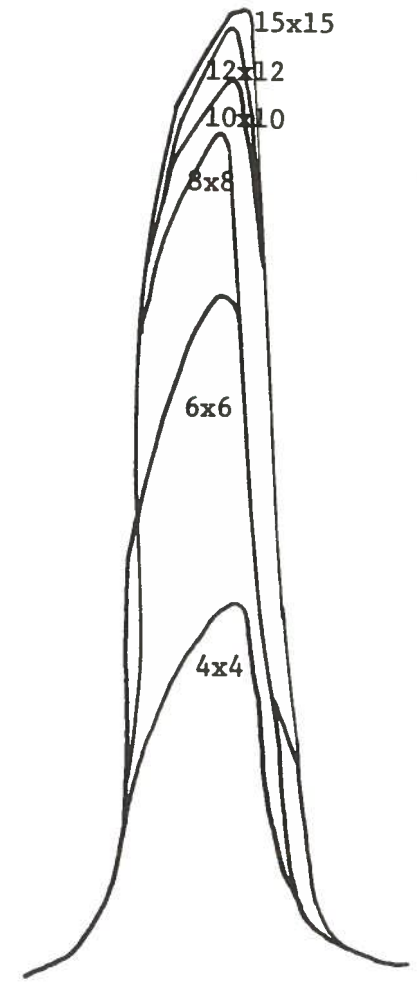

Figure 11. Beam profiles for 6 MeV electrons with the 2.5 cm contact cone. All plots referenced to 15x15 plot.

Due to the similarity of the 15x15 to the 12x12 cm and the 10x10 to the 8x8 cm beam profiles, the 15x15 and the 10x10 cm collimator settings were used for the remainder of the collimator test. The 4x4 cm beam profile was not used because of its low output as compared to the rest of the beam profiles. Therefore, the remainiing contact cones beam profiles were plotted for a 15x15, 10x10, and a 6x6 cm collimator setting for each energy. Because the 10x10 collimator profiles were more uniform, the 10x10 cm setting was chosen to be used for the remainder of the study (Figure 12).

The percent depth dose curves seen in Figure 13 were determined from the relative ionization data obtained with the PTW ion chamber and water phantom. It is accepted practice (Tapley 1976) to correct for 3/4 of the ion chamber radius. Because the initial polarity test showed a variation of less than 1% between the negative and positive positions, it was not necessary to take readings at both polarities. The data from the percent depth dose curves were compared with the isodensity curves to produce the isodose curves represented in Figure 14 for all the contact cones at each energy. This comparison means that each isodensity curve is at a corresponding depth (90% isodensity equals 90% depth dose) as determined from the percent depth dose curve. All the isodose curves were normalized to a maximum density reading (i.e. 100%).

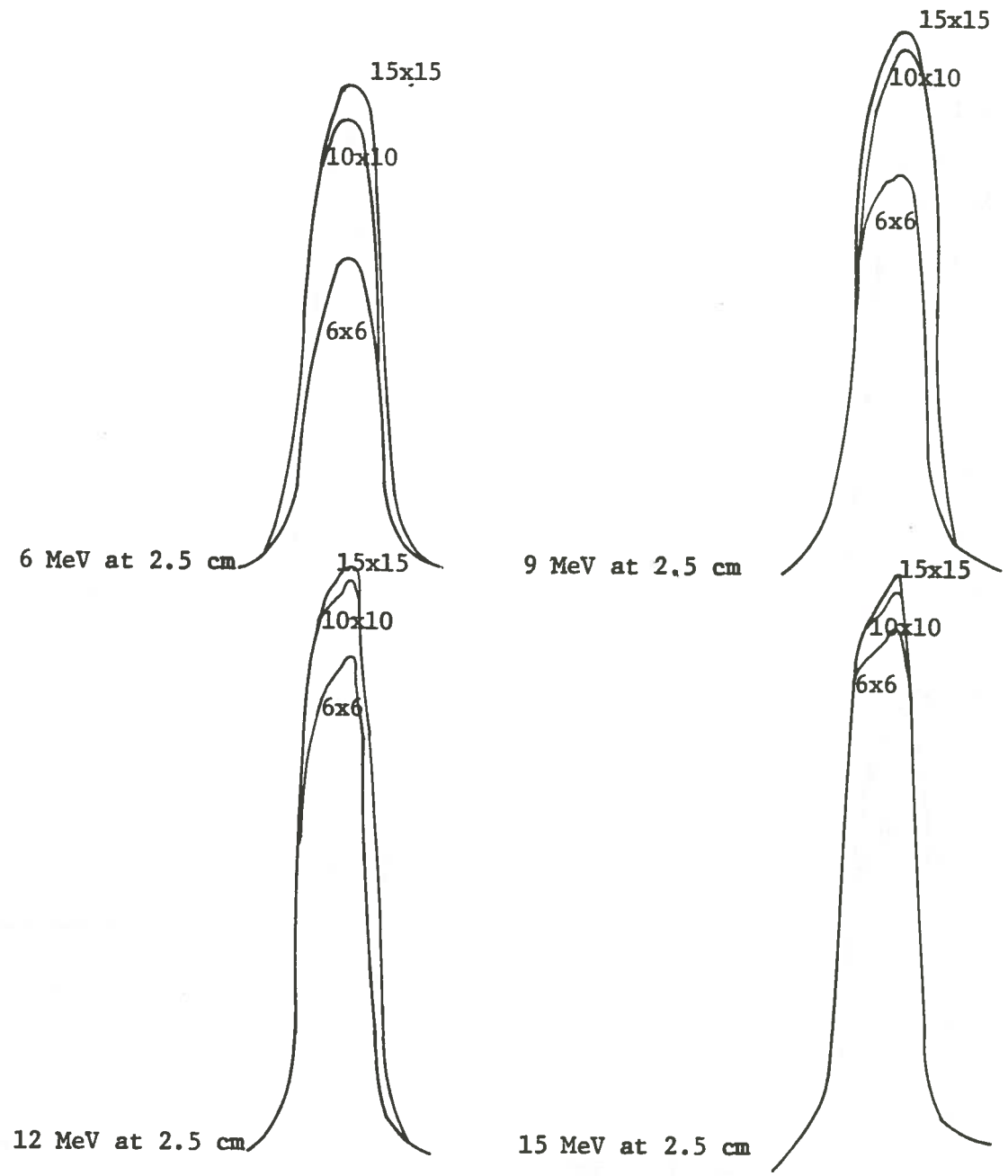

Figure 12.1 Beam profiles. All plots referenced to 15x15.

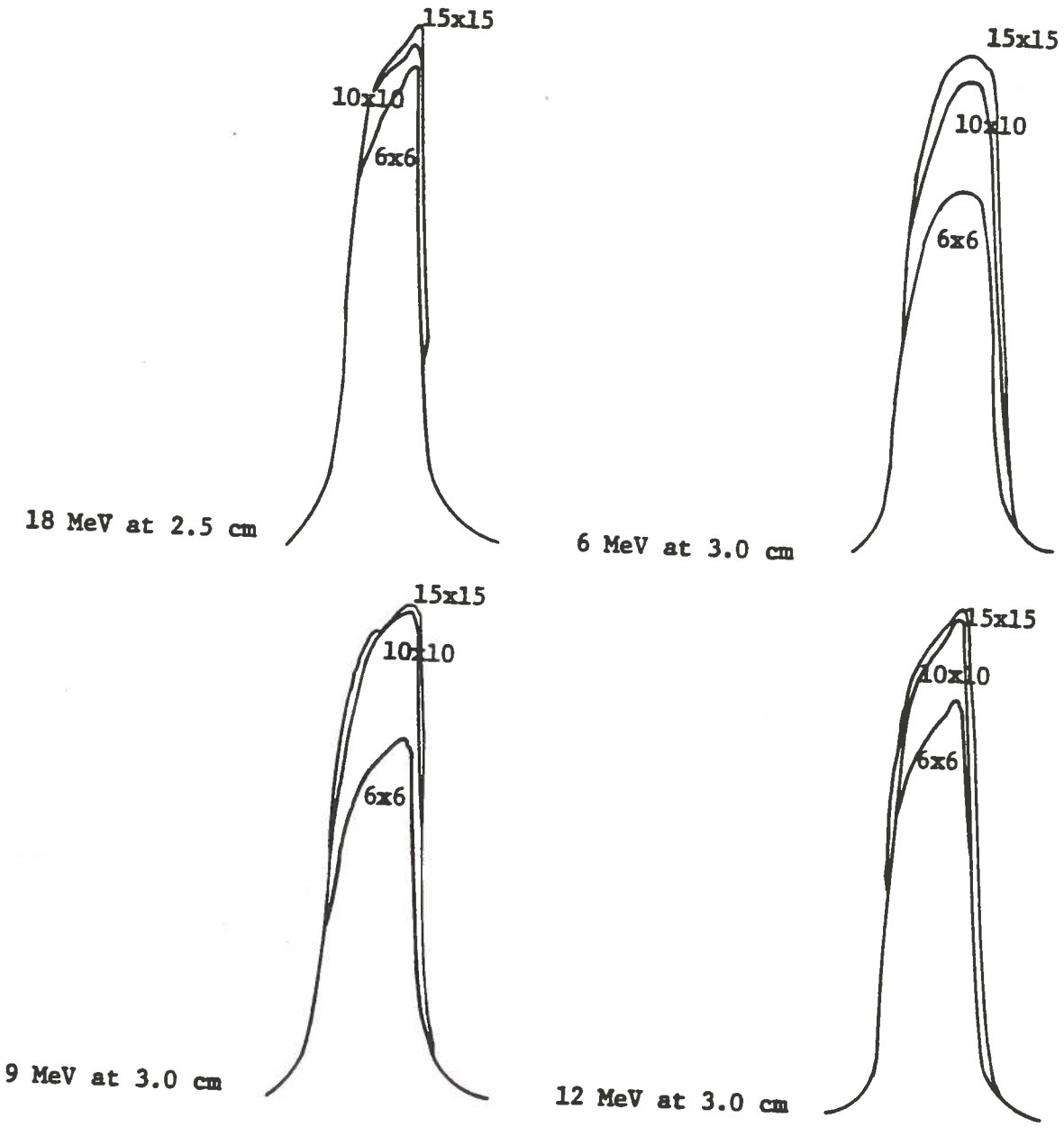

Figure 12.2 Beam profiles. All plots referenced to 15x15.

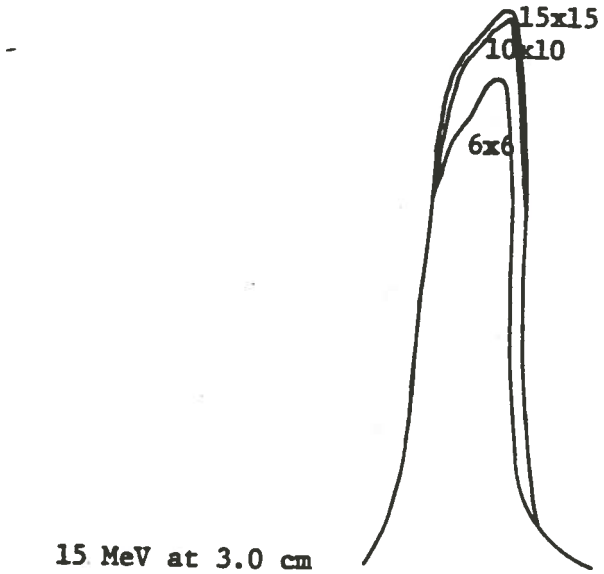

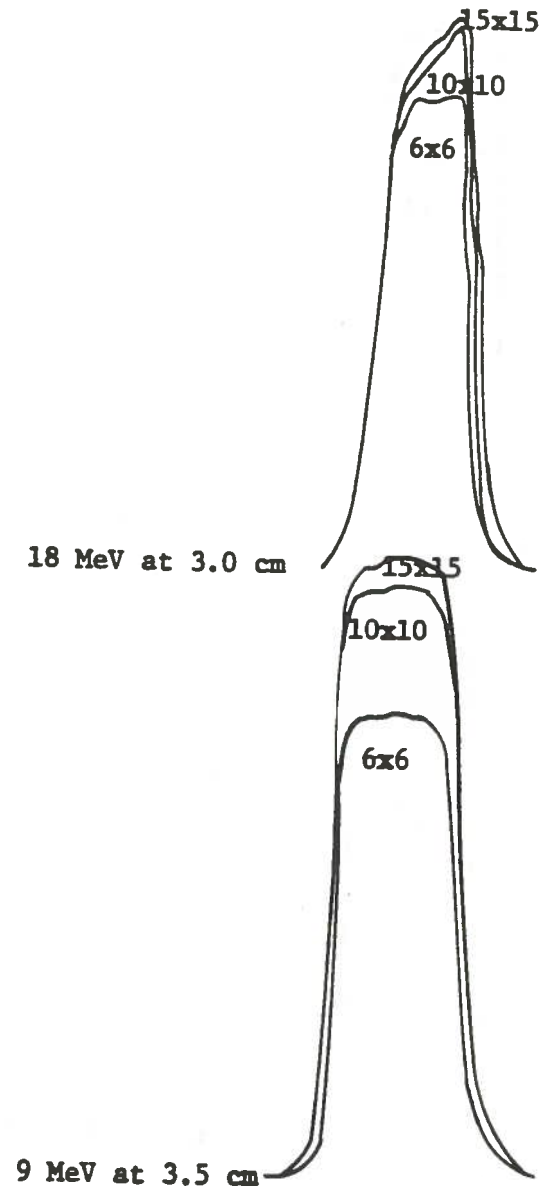

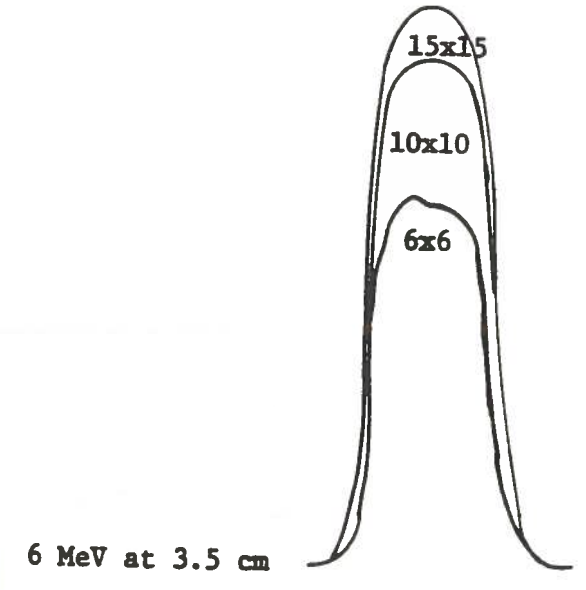

Figure 12.3 Beam profiles. All plots referenced to 15x15.

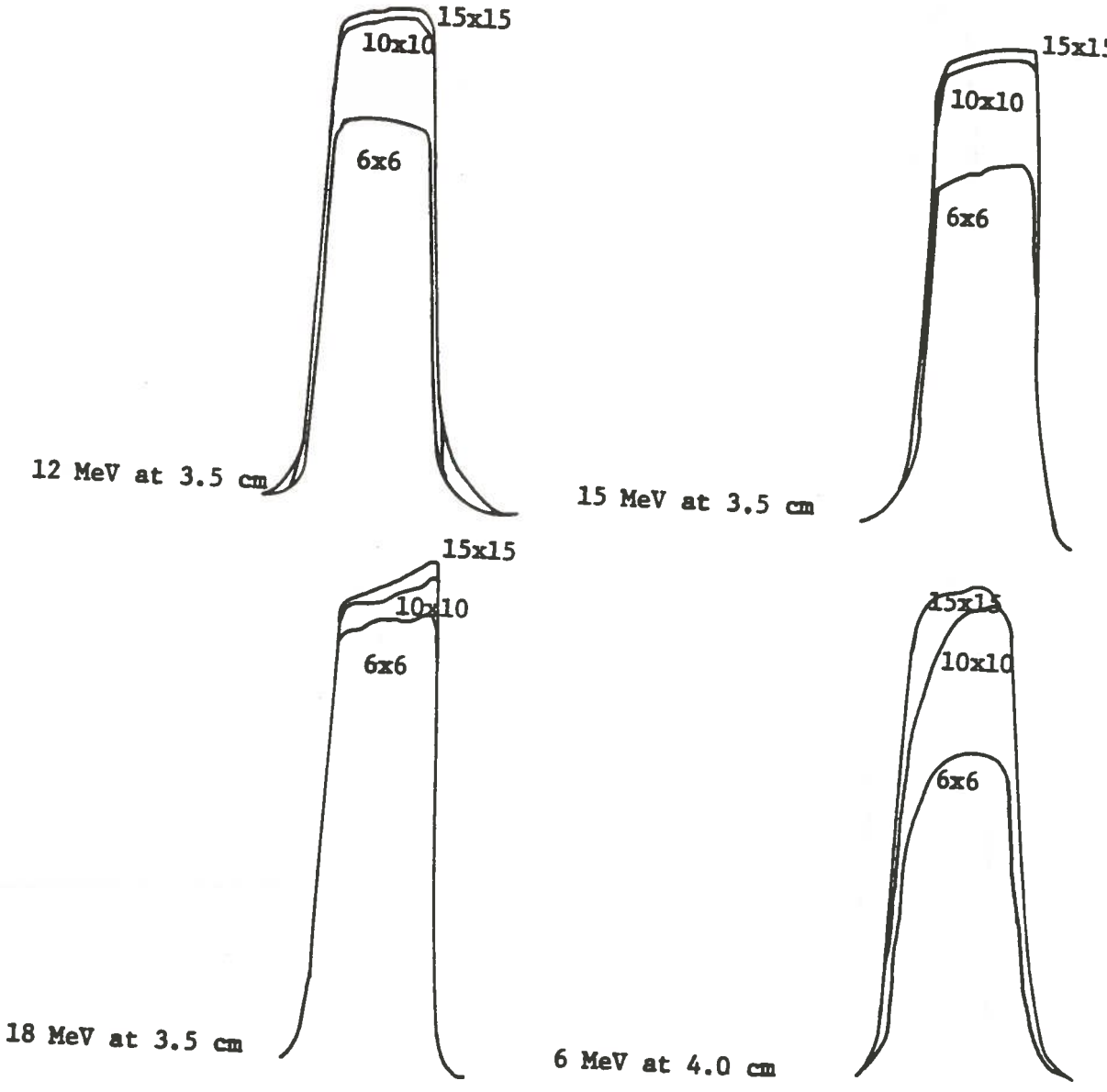

Figure 12.4 Beam profiles. All plots referenced to 15x15.

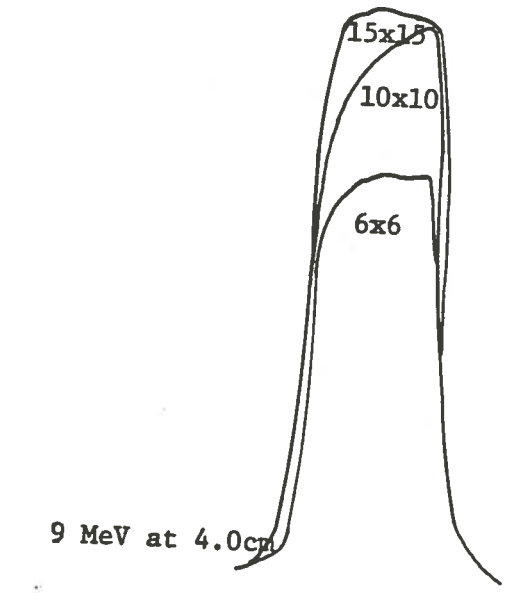

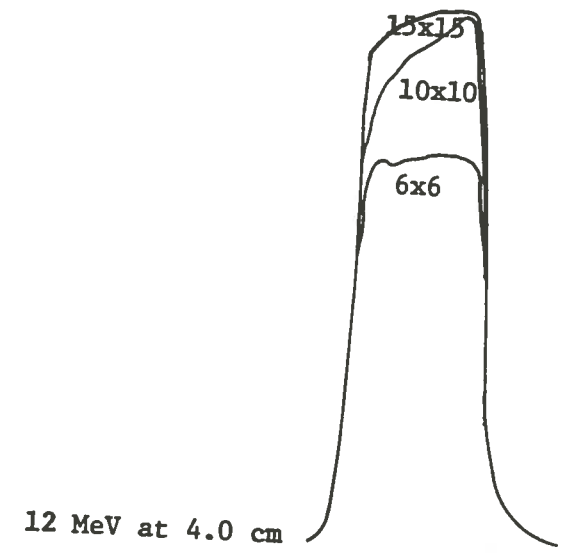

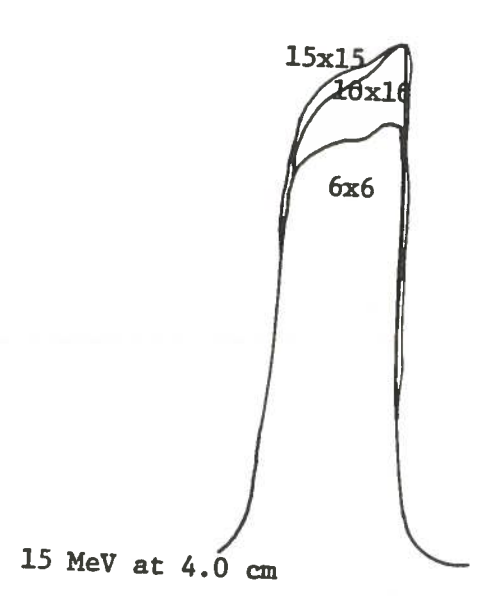

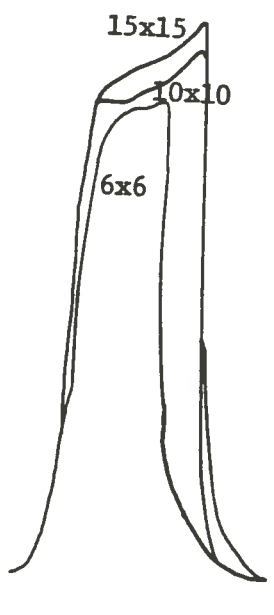

Figure 12.5 Beam profiles. All plots referenced to 15x15.

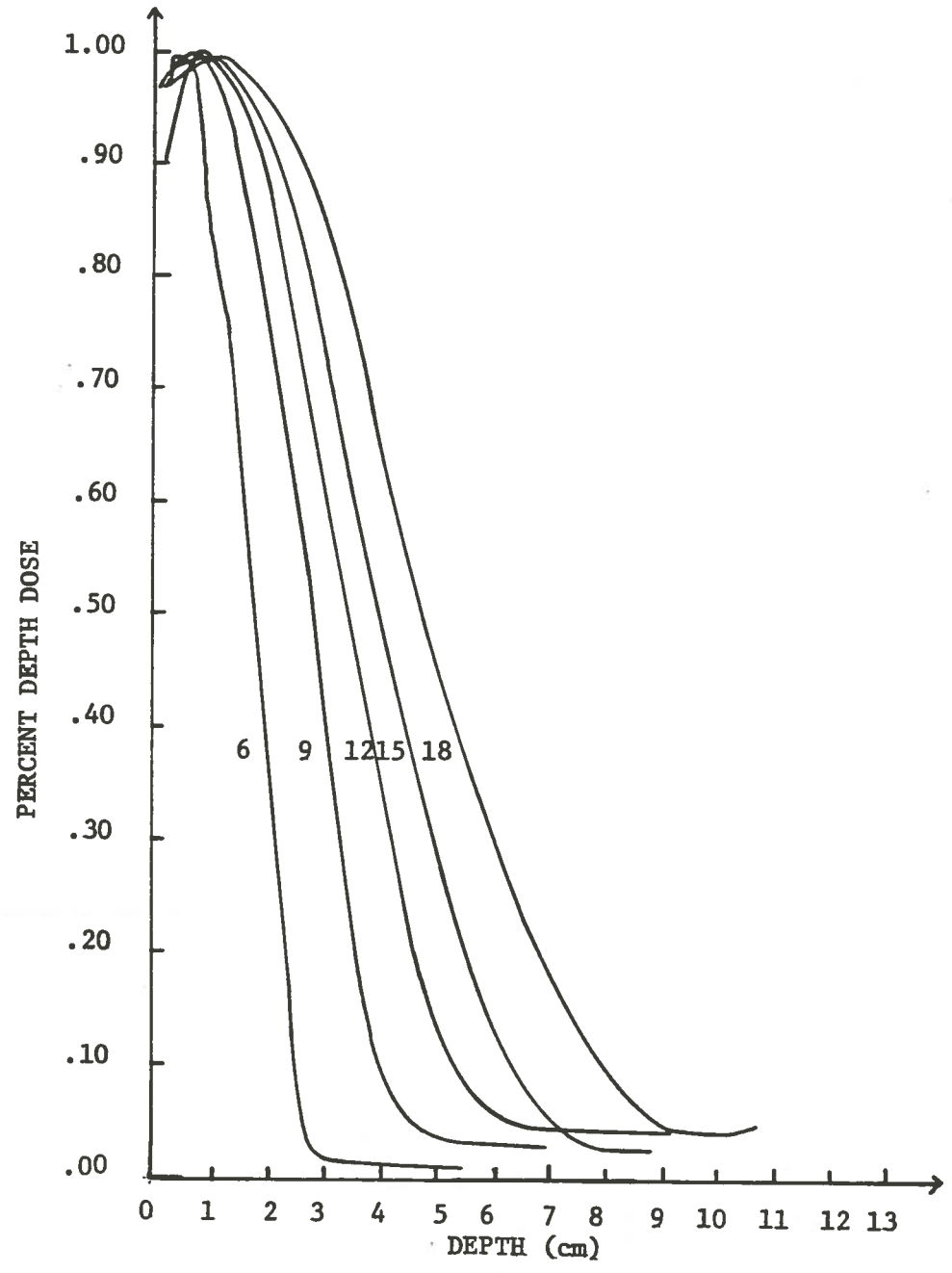

Figure 13.1 Percent depth dose curves for 2.5 cm contact cone at 6, 9, 12, 15, and 18 MeV electron energies.

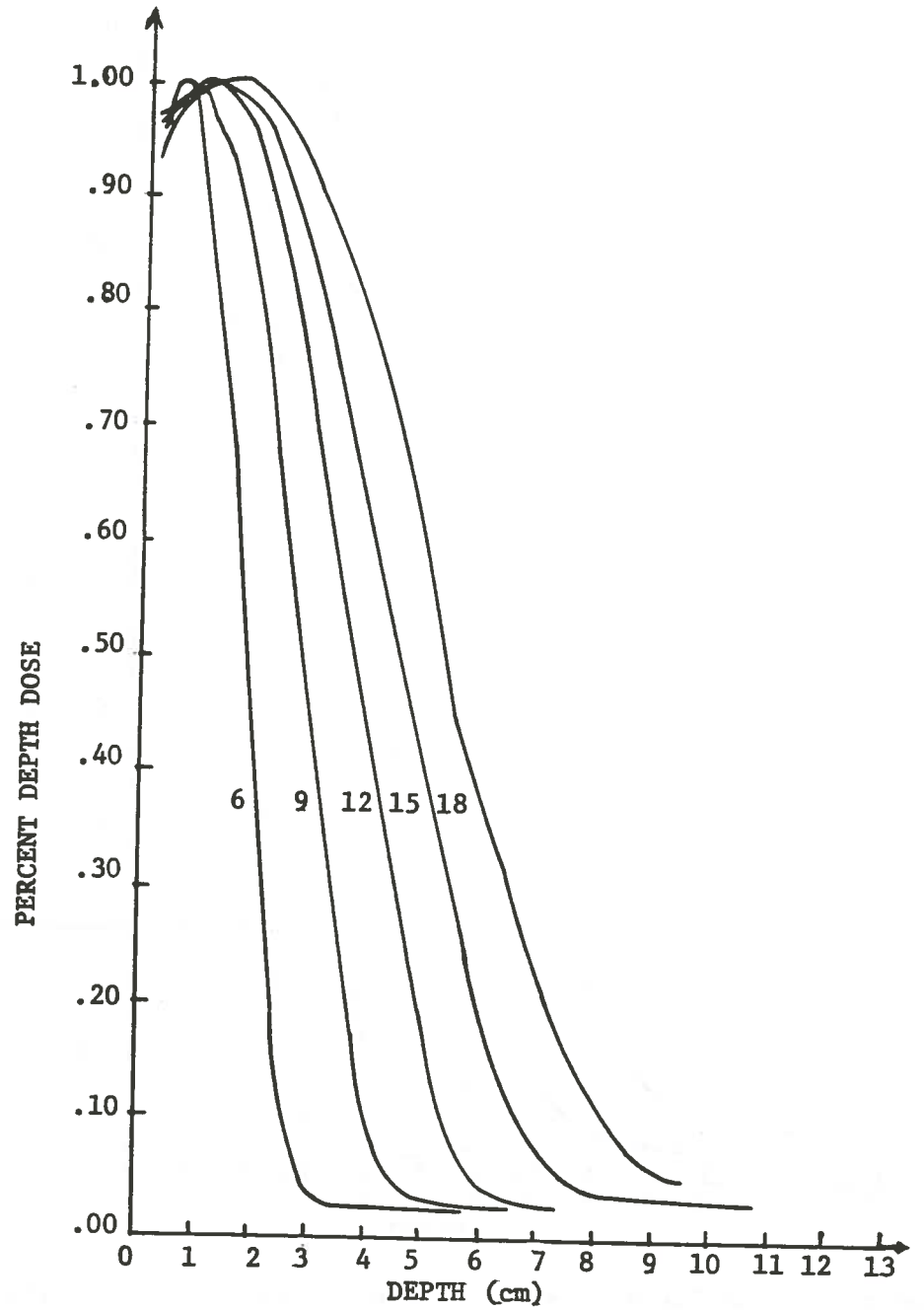

Figure 13.2 Percent depth dose curves for 3.0 cm contact cones at 6, 9, 12, 15, and 18 MeV electron energies.

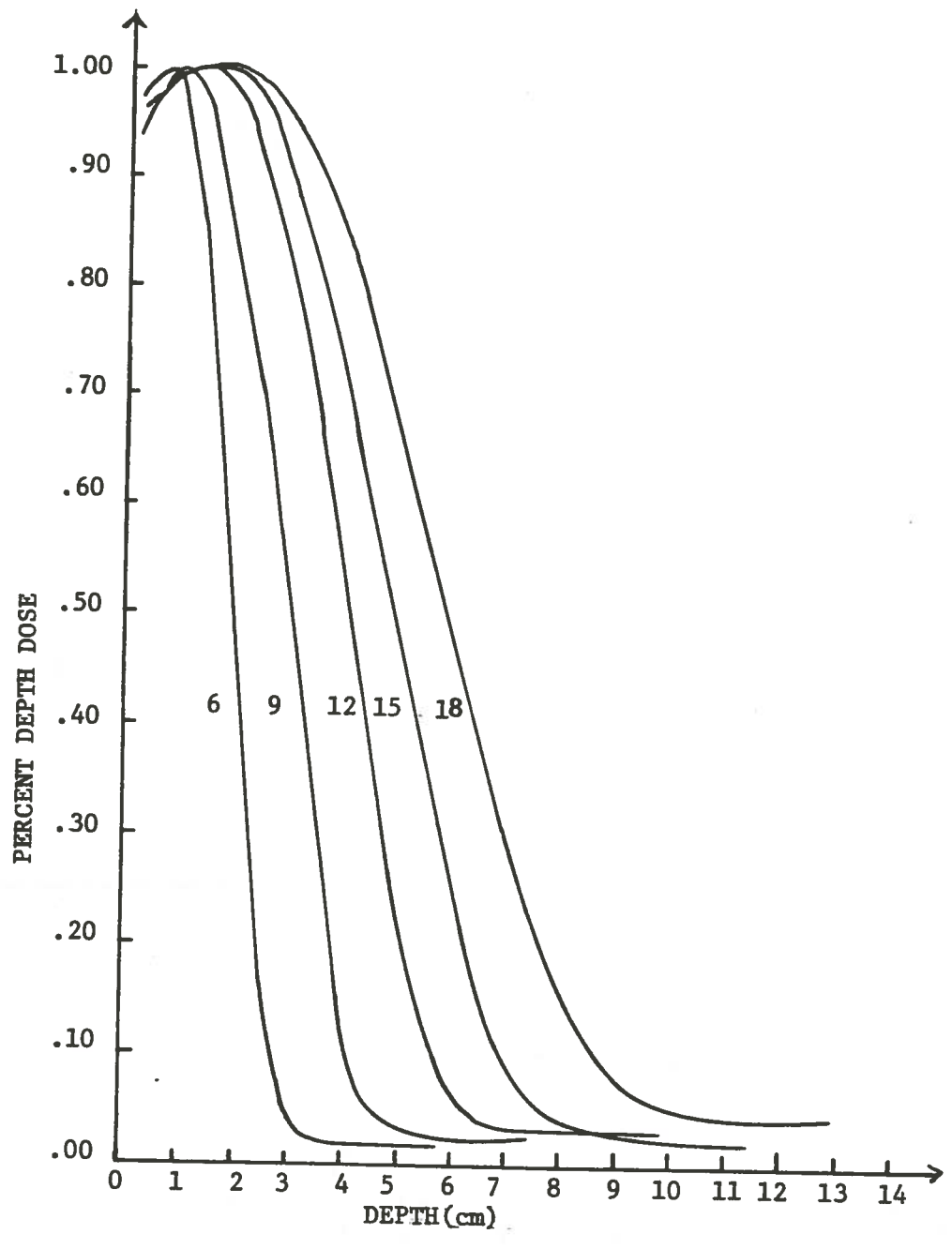

Figure 13.3 Percent depth dose curves for 3.5 cm contact cone at 6, 9, 12, 15, and 18 MeV electron energies.

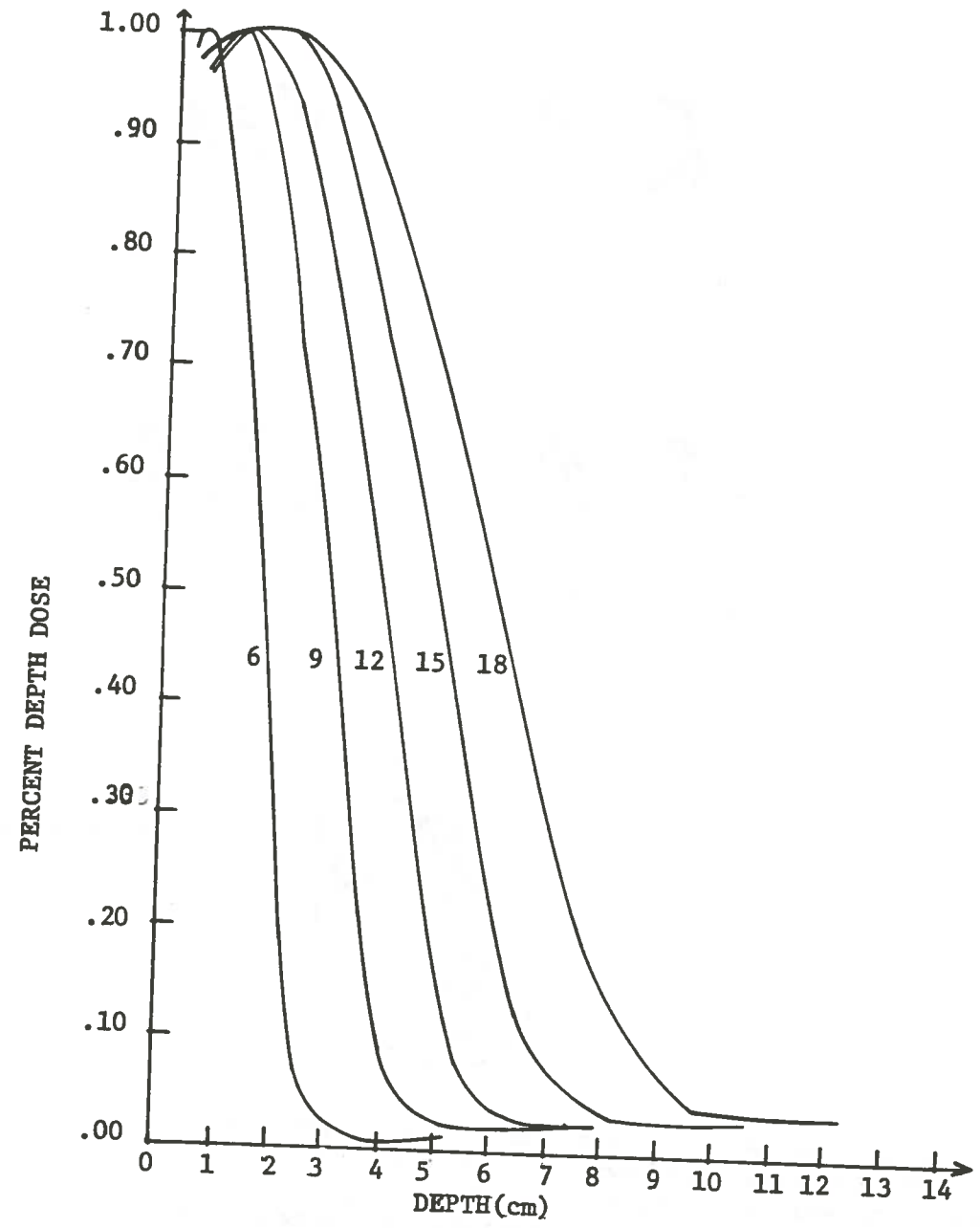

Figure 13.4 Percent depth dose curves for 4.0 cm contact cone at 6, 9, 12, 15, and 18 MeV electron energies.

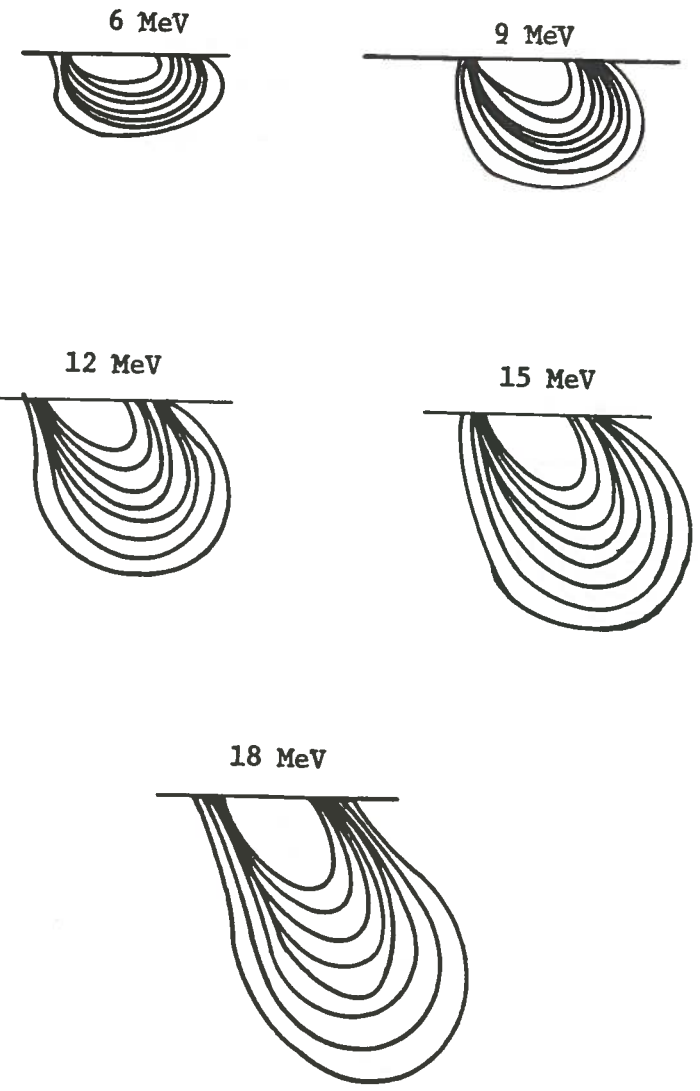

Figure 14.1 Isodose curves for 2.5 cm contact cone at varying beam energies. Each successive curve represents 90%, 80%, 70%, 60%, 50%, 40%, 30%, 20%, of the dose relative to dose maximum starting with the innermost curve.

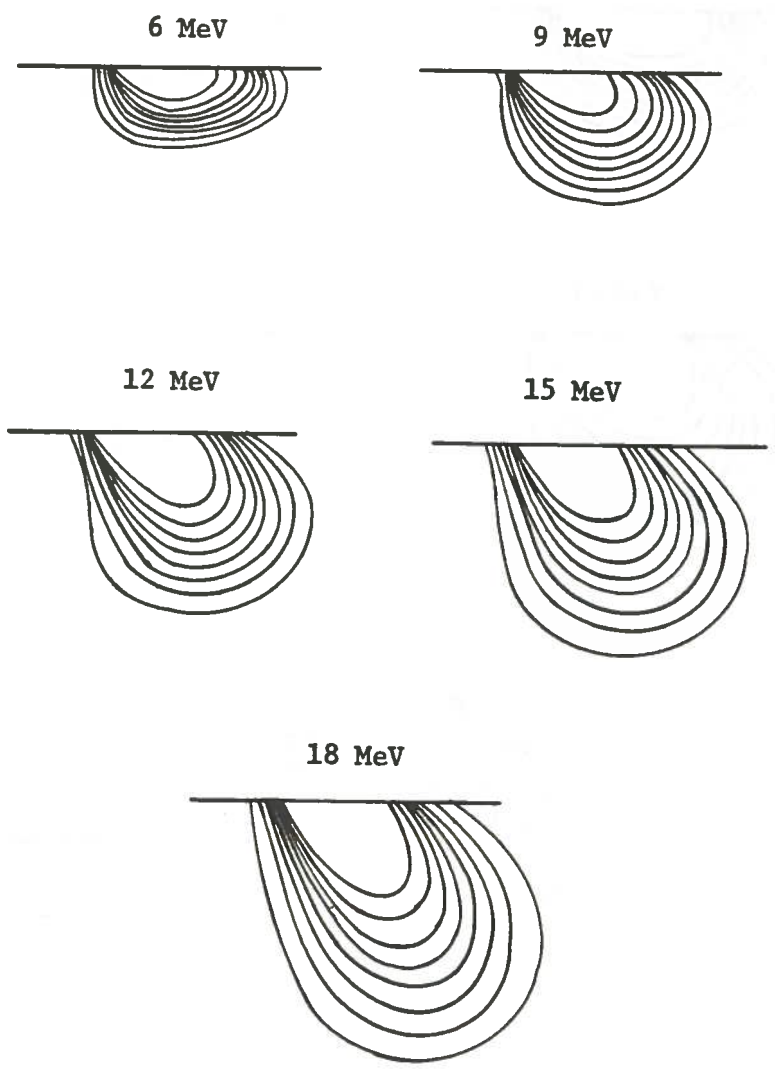

Figure 14.2 Isodose curves for 3.0 cm contact cone. See legend figure 14,1.

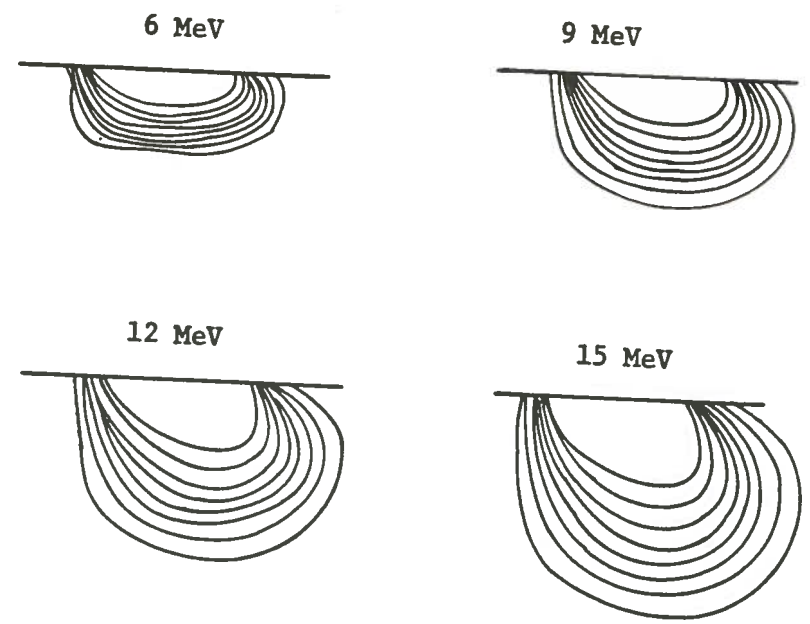

Figure 14.3 Isodose curves for 3.5 cm contact cone. See legend figure 14.1.

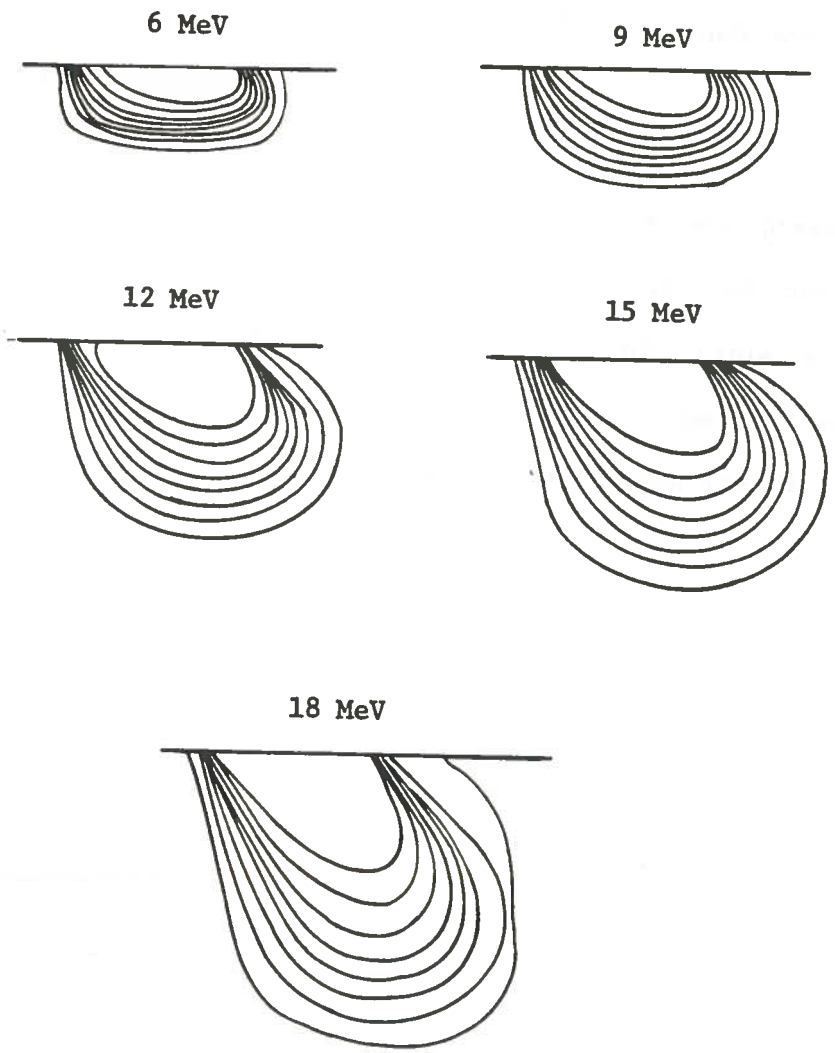

Figure 14.4 Isodose curves for 4.0 cm contact cone. See legend figure 14.1.

The range of electrons, the energy of the beam at the surface of the phantom, and the percentage of photon contamination were determined from the relative ionization data following recommendations of ICRU Report #21. The energy, the range, and photon contamination all increased as the energy increased for each contact cone size (Table 1).

The calibration data or output factors are presented in Table 2. These represent the number of rad delivered per monitor unit at dose maximum. The values given in this table are intended to be applied to dose calculations for patients being treated with the contact cones available at the Perkins Radiation Treatment Center.

TABLE 1. Data determinend from the relative ionization curves.

Cone Diameter (cm)	Energy (MeV) Ea	Energy (MeV) Eo	Range of Dose Maximum (cm)	Range of Electrons (cm)	Photon Contamination (%)
2.5	6	5.32	0.36	2.55	1.3
"	9	8.50	0.86	4.05	3.2
"	12	10.71	1.16	5.20	4.8
"	15	12.53	1.26	6.15	3.4
"	18	14.45	1.16	7.15	3.5
3.0	6	5.81	0.56	2.65	2.4
"	9	8.40	0.86	4.00	2.8
"	12	11.09	1.16	5.40	3.0
"	15	13.20	1.26	6.50	3.5
"	18	15.70	1.67	7.80	4.5
3.5	6	5.81	0.86	2.65	1.9
"	9	8.69	1.06	4.15	2.5
"	12	11.95	1.56	5.85	2.6
"	15	14.26	1.96	7.05	2.6
"	18	16.60	1.96	8.25	4.2
4.0	6	5.52	0.50	2.50	1.0
"	9	8.50	1.05	4.05	2.2
"	12	11.09	1.25	5.40	3.0
"	15	13.39	1.85	6.60	3.0
"	18	16.56	2.15	8.25	3.7

Ea = Energy at accelerator window (nominal)

Eo = Energy at the surface of the phantom

Missing in page number only.

Table 2. Contact cone calibration factors. Each value represents the number of rad delivered per monitor unit at dose maximum. Collimator setting at 10x10 cm.

Contact Cone Diameter (cm)	Energy (MeV)				
	6	9	12	15	18
2.5	.583	.736	.810	.844	.876
3.0	.670	.819	.871	.896	.919
3.5	.639	.798	.860	.883	.918
4.0	.685	.840	.902	.915	.937

CONCLUSION

Contact cones have been used throughout the history of radiotherapy to treat cancer. The contact cone system at Perkins Radiation Center is a versatile method of treating cancer. From the results shown in this report, the contact cones should be used with a 10x10 cm collimator setting. This particular setting gives the best overall beam profile. With a 10x10 cm collimator setting, any cone diameter at any energy will produce a similar beam profile. This similarity or reproducibility of the beam profile allows the contact cones to be interchangable.

One of the most important results of this experimental work is the percent depth dose curve. From the data in Table 1, it can be seen that the initial energy of the beam (energy listed on the control board) is higher (as much as 25%) than the energy at the end of the cone. This lower energy causes a shallower maximum dose to occur in the phantom. Therefore, the percent depth dose curves are unique for these contact cones on this type of linear accelerator.

The range of the electrons from the contact cones is also a unique characteristic of these cones. The range of the electrons is dependent upon the cone diameter and the energy used. With a difference in the range of 6 cm (2.5 cm at 6 MeV is 2.55 cm while

4.0 cm at 18 MeV is 8.25 cm), the range of the electrons should be examined before a particular contact cone is used.

The photon contamination, as listed in Table 1 is fairly small. The worse case occurs with the 3.0 cm at 18 MeV 4.5% and this is negligible. The low value of 1.0% for 4.0 cm at 6 MeV is due to calculation error. This value was estimated from the appropriate relative ionization curve.

From the isodose curves, the 30 degree bevel of the contact cones is obvious. This "slant" on the end of the cone causes the isodose curves to be slightly peaked toward the tip of the cone (the longest dimension) as seen in Figure 14.

The purpose of this thesis was to provide clinically significant data for the contact cone system in use at Perkins Radiation Treatment Center. Although the end results are the calibration factors, the percent depth dose curves and the isodose curves can provide great insight to the physician. The ability to see how the contact cones are affecting the electron beam inside the medium can increase the technical ability of the physician to design a better regimen for the treatment of cancer.

REFERENCES

Abe, M. et al. 1975. Techniques, indications and results of intraoperative radiotherapy of advanced cancers. Radiology. 116.

Abe, M. and Takahashi, M. 1981. Intraoperative radiotherapy: the Japanese experience. Int. J. Radiat. Oncol. Biol. Phys. 7.

Briggs, P. and Wang, C. 1984. Breakaway safety features for an intraoral cone system. Inter. J. Radiat. Oncol. Biol. Phys., 9.

Del Regato, J. 1948. The role of transvaginal roentgentherapy in the treatment of carcinoma of the cervix. Surg., Gynec., and Obst. 86.

Del Regato, J. 1952. Integral roentgen therapy for carcinoma of the cervix uteri. Presented at American Roentgen Ray Society, Houston, TX. 1952.

Fairchild, G. and Shorter, A. 1947. Irradiation of gastric cancer. Br. J. Radiol. 20.

Fayos, J. and Lampe, I. 1967. Radiotherapy of squamous cell carcinoma of the oral portion of the tongue. Arch. Surg. 94.

Griffin, T. et al. 1977. Peroral irradiation for limited carcinoma of the oral cavity. Int. J. Radiol. Oncol. Biol. Phys. 2.

Hiroake, T.; Nakagawa. I.; and Tashiro, S. 1975. Intraoperative irradiation therapy for unresectable pancreatic cancer. Nippon Gan Chiryo Gakkai Shi. 13.

International Commission on Radiation Units and Measurements (ICRU). 1971. Radiation dosimetry: electrons with initial energies between 1 and 50 MeV. ICRU Publication, Washington, D.C.

Metzger, U.; Kisner, D.; and Ghosh, B. 1983. Combined modality treatment of pancreatic cancer: implications for the surgeon. Journal of Surgical Oncology. 24.

Nolan, J. 1960. Response of carcinoma in situ of the cervix to radiation therapy. Am. J. Obst. and Gynec. 79.

Phillips, T., 1968. Peroral roentgen therapy. Radiology. 90.

Rich, T. et al. 1984, Orthovoltage intraoperative radiotherapy: a new look at an old idea. Int. J. Radiat. Oncol. Biol. Phys. 10.

Scaramucci, J.; Fennel, R.; and Hepp, J. 1958. Carcinoma in situ of the cervix. A report of fity-one cases, with consideration of minimal therapy. Obst. and Gynec. 12.

Swindell, W. 1983. An endocavitary irradiator: two modifications for improved utility. Int. J. Radiat. Oncol. Biol. Phys. 9.

Tapley, N. ed. 1976. Clinical applications of the electron beam. John Wiley and Sons, New York, NY

Wang, C. 1980. Treatment of oral cancer by intra-oral cone - results and complications. Presented at the Annual Meeting of the New England Society of Radiation Oncologists, Newport, RI.

Watson, T. 1943. Subcutaneous x-ray therapy. Br. J. Radiol. 13.

White, C. 1983. A methodological evaluation of the energies in degraded electron beams. Louisiana State University, M.S. Thesis.

Wilenzick, R., et al. 1983. Evaluation of a commercial applicator system for intraoperative radiotherapy. Personal Communication.

Wood, W. et. al. 1981. Intraoperative radiation for unresectable pancreatic carcinoma. Proc. Am. Soc. Surg. Oncol. 34.

MASTER'S EXAMINATION AND THESIS REPORT

Candidate: William Tyrone Fontenot

Major Field: Nuclear Science (Medical Radiation Science Option)

Title of Thesis: Beam Characteristics Of Contact Cones For Use In Endocavitary Irradiation

Approved:

Major Professor and Chairman

Dean of the Graduate School

EXAMINING COMMITTEE:

Date of Examination:

April 30, 1985

Figure 16.1 The effect of angular errors was also dependent upon cone diameter for the beveled cones.

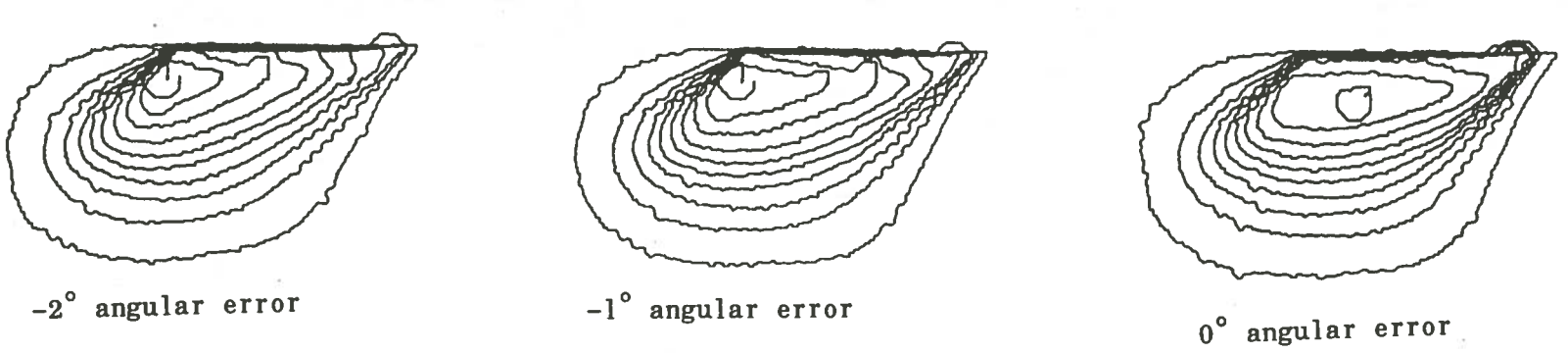

Isodensity curves generated from film exposed with 9 MeV electrons utilizing the 3.0 cm 45° beveled cone (above) and the 5.0 cm 45° beveled cone (below). Note that angular errors of minus 1 or 2 degrees had little or no effect when the larger cone was employed.

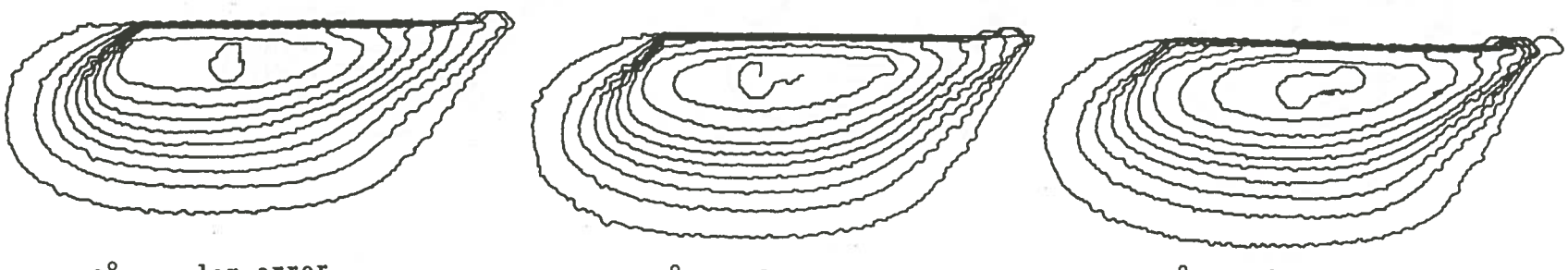

Figure 16.2 Regarding the beveled cones, angular errors in the plus direction also produced greater effects when the smaller cone was used.

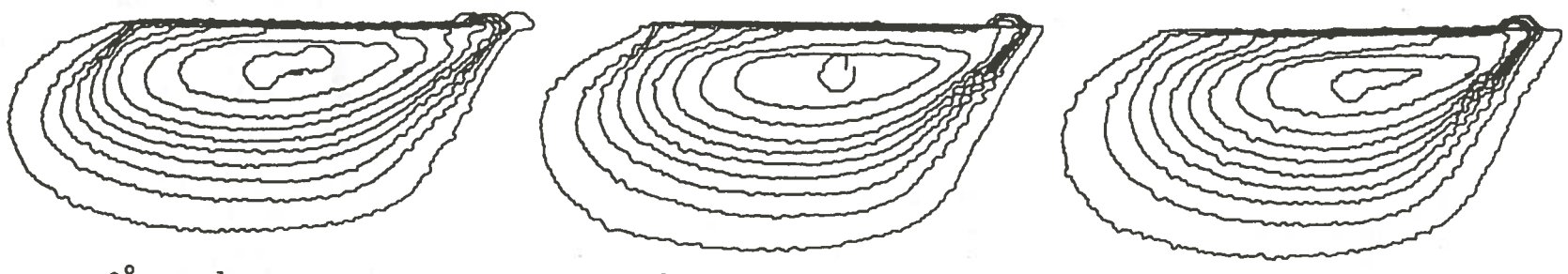

0° angular error +1° angular error +2° angular error

Isodensity curves generated from film exposed with 9 MeV electrons utilizing the 5.0 cm 45° beveled cone (above) and the 3.0 cm 45° beveled cone (below). Errors of plus 1 or 2 degrees produced little or no effect when the larger cone was employed.

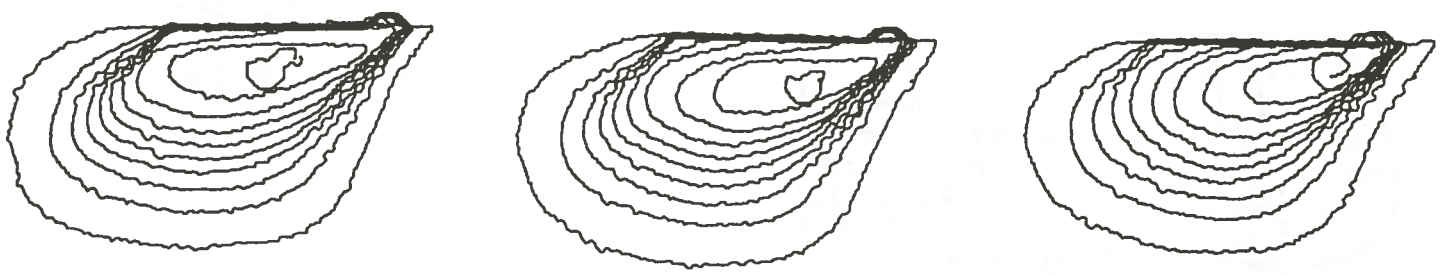

0° angular error +1° angular error +2° angular error

Figure 17. Illustrates the energy dependence of the effects.

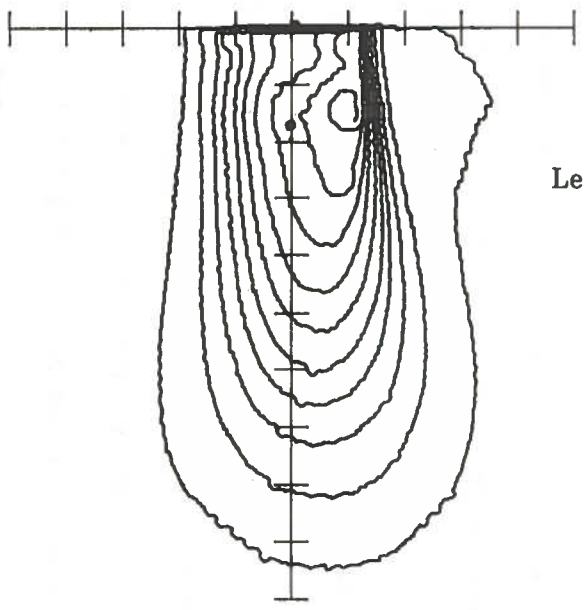

Left: With a 3° angular error, the optical density at d_{max} was greater than the 80% line when 20 MeV electrons were applied with the 3.0 cm non-beveled cone. The point on the curves designates d_{max}.

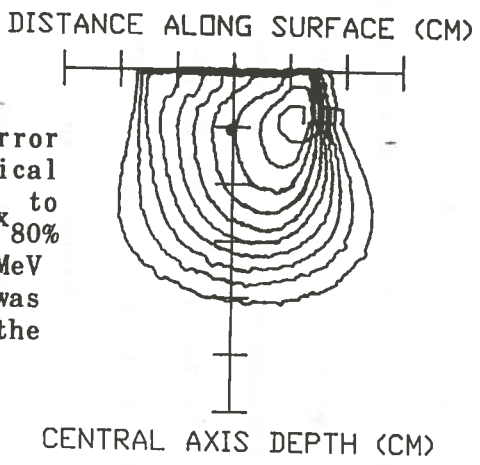

Right: A 3° angular error caused the optical density at d_{max} to fall below the 80% line when a 9 MeV electron beam was employed with the same cone.

when a 20 MeV electron beam was used with the 3.0 cm non-beveled cone. But the same gantry error caused the optical density at d_{max} to fall below the 80 percent line when the same cone was employed with a 9 MeV electron beam. But the energy dependence diminished with the larger cones (Figure 18). Figure 19 demonstrates that the effect of angular errors was also energy dependent when the beveled cones were employed.

The dose along the central axis fell off more rapidly with increased angular errors. Although this was apparent on the isodensity curves, some central axis depth-density curves are presented in Figure 20 to more accurately depict the increased falloff of dose.

With angular errors, the central axis intensity was reduced due to redirection of the original central axis, and electrons traveling parallel to it, into the distal side of the cone, therefore causing attenuation. This is represented in Figure 21 with a 5° angular error. In this diagram one can see that electrons traveling on the proximal side of the beam are directed away from the cone wall, resulting in a reduction in dose on that side of the beam axis.

The dependence upon cone diameter is analogous to the effect of field size on the significance of penumbra in a ^{60}Co beam. Just as the penumbra is more significant with small x-ray field sizes, so are the side-scattered electrons more significant with the smaller cones.

The Phantoms Compared

An electron beam is almost monoenergetic before hitting the accelerator window, but the energy is degraded as it passes through the window, the scattering foil, the monitor chamber, etc. (Khan, 1984). By the time the beam hits the phantom surface it has taken on a spectrum of

Figure 18. Isodensity curves which demonstrate that the energy dependence diminished with the larger cones.

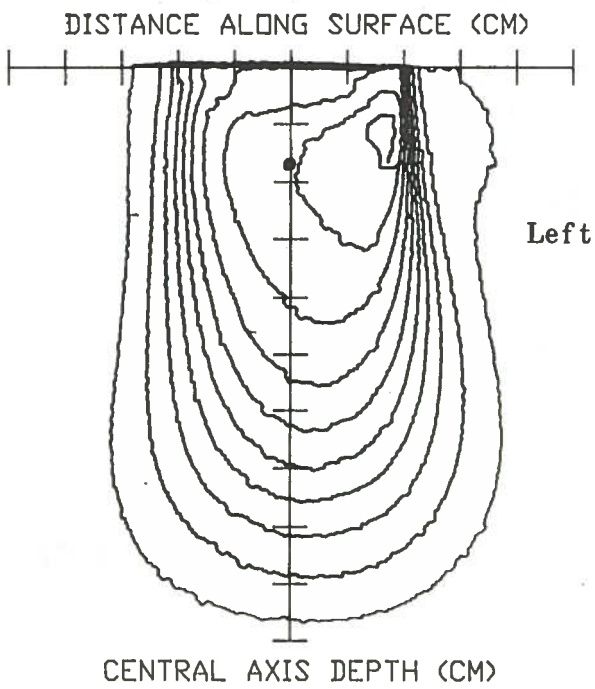

Left: With a 3° angular error the optical density at d_{max} was close to, but less than, the 90% line when 20 MeV electrons were applied with the 5.0 cm non-beveled cone.

Right: With a 3° angular error the optical density at d_{max} was also close to, but less than, the 90% line when 9 MeV electrons were applied with the same cone.

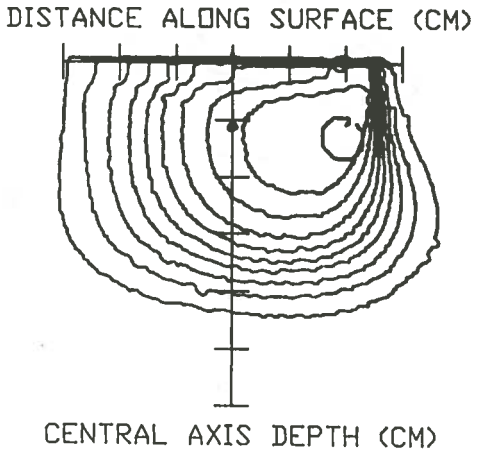

Figure 19. Isodensity curves which demonstrate that the effect was energy dependent when the beveled cones were employed.

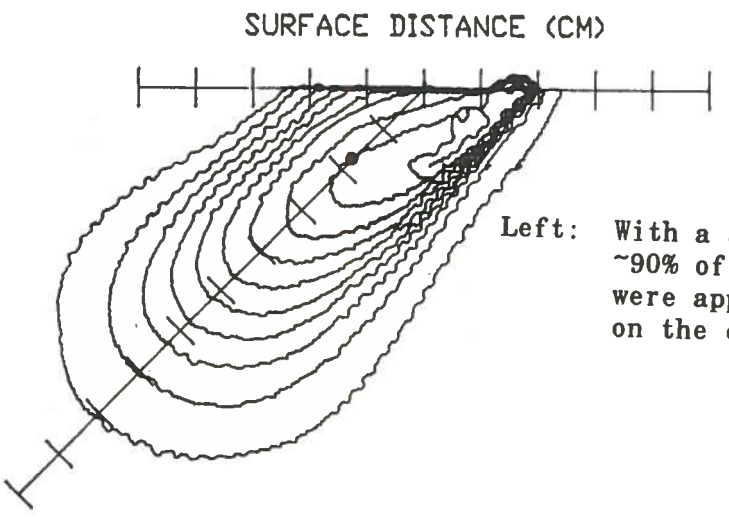

Left: With a 3° angular error, the optical density at d_{max} was ~90% of the maximum optical density when 16 MeV electrons were applied with the 3.0 cm 45° beveled cone. The point on the curves designates d_{max}.

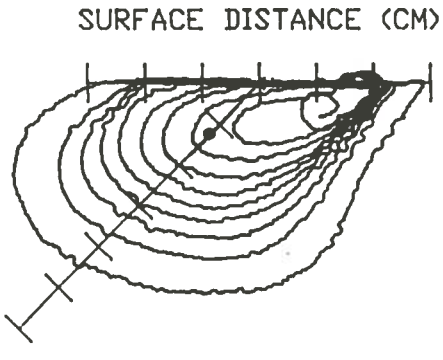

Right: A 3° angular error caused the optical density at d_{max} to fall well below the 90% line when a 9 MeV beam was employed with the same cone.

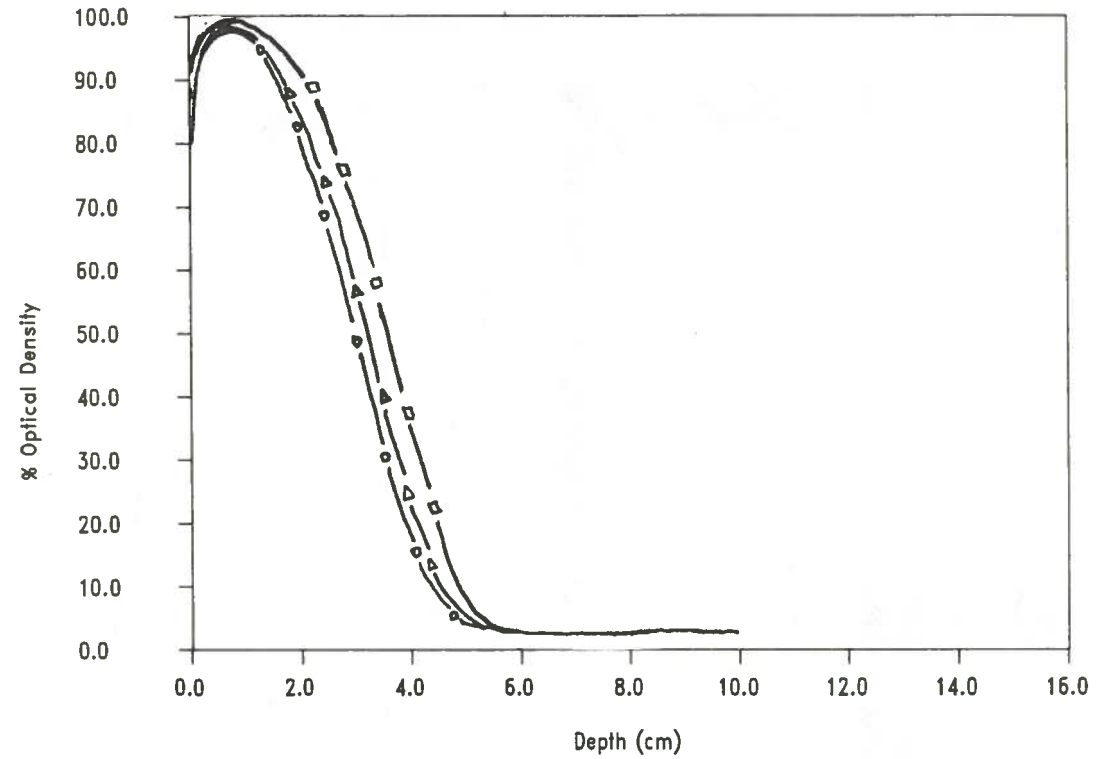

□ gantry vertical

Δ 3° angular error

O 5° angular error

Figure 20. Central axis depth-density curves generated from film irradiated with 9 MeV electrons using the 5.0 cm non-beveled cone. Depicts an increased falloff in dose with increased angular errors.

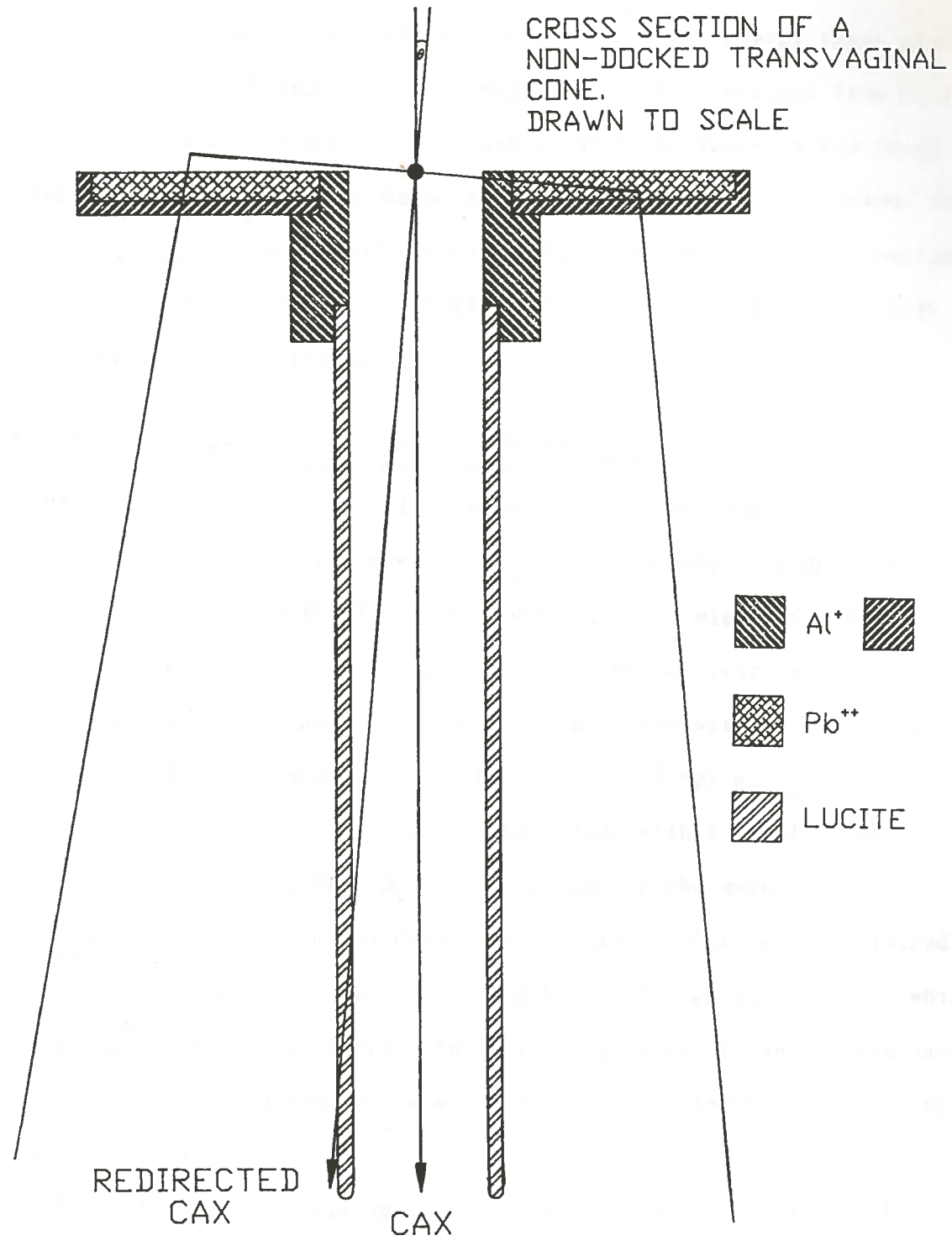

Figure 21. Illustrates redirection of the original central axis into the distal side of the cone with a 5° gantry error. $\theta=5^{\circ}$

energies, and "further degradation and spread of beam energy takes place with depth in the phantom" (Khan, 1984). Using data obtained from film, the degradation of the beam within each phantom was compared and found to differ insignificantly. The data comparing the two phantoms include the d_{max}, d_{50}, d_{80}, R_p (practical range) and $\overline{E}_0$ (mean energy of the beam)and are presented in Table 2. Figure 22 presents a depth-dose curve which illustrates the definition of R_p.

The Effect of Angular Errors on the Dose at d_{max}

According to the results in this portion of the study, the effect of angular setup errors on the dose at d_{max} depended most critically on the cone diameter, less critically on the energy of the electron beam, and in the case of beveling, on the direction in which the error was made. If the cone was too small and the energy too low, even with no beveling, errors as small as 3° substantially decreased readings at d_{max}. The situation was worsened in the case of beveling; with a bevel of 45°, errors as small as 1° were significant if made in the more crucial direction, i.e., in the minus direction. In spite of a few unexplained inconsistencies, general trends were exhibited throughout the study which support the conclusions stated. In this study, a signficant effect was said to have occurred when there was a reduction in the dose at d_{max} by 5 percent or more.

Regarding the non-beveled cones, no significant reduction in the readings at d_{max} occurred until at least 3° error. But when the smallest cone was employed, a 3° angular error produced a substantial decrease in the reading regardless of the energy of the beam (see Table 3 for percentages). However, the effect was somewhat dependent upon the

Table 2

Data Comparing the Masonite and Polystyrene Phantoms*

Phantom	Energy (MeV)	d_{max} (cm)	d_{50} (a) (cm)	d_{80} (b) (cm)	R_p (c) (cm)	$\bar{E}_0$ (d) (MeV)
Polystyrene	20	2.5	8.0	5.7	10.9	18.7
Masonite	20	2.5	7.8	5.9	10.8	18.0
Polystyrene	16	2.2	4.7	6.2	8.8	14.4
Masonite	16	2.0	4.9	6.4	8.9	14.9
Polystyrene	12	1.7	3.6	4.4	5.8	10.4
Masonite	12	1.7	3.7	4.7	6.1	10.7
Polystyrene	9	1.4	2.8	3.4	4.3	7.9
Masonite	9	1.3	2.9	3.5	4.5	8.0

(a) d_{50} is the depth at which the dose is 50% of the maximum dose

(b) d_{80} is the depth at which the dose is 80% of the maximum dose

(c) The R_p is "the depth of the point where the tangent to the descending linear portion of the curve at the point of inflection intersects the extrapolated background" (Khan, 1984)

(d) The mean energy of the beam was determined by using the following relationship:

$$\bar{E}_0 = C \bullet d_{50} \text{ where } C = 2.33 \text{ MeV cm}^{-1}$$

for water (Khan, 1984; Wu et al., 1984)

* These data were obtained from central axis depth-density curves each prepared from a separate film exposed in either the masonite or polystyrene phantom. A film was irradiated by each electron energy with the gantry accurately aligned, using the 4.3 cm non-beveled cone.

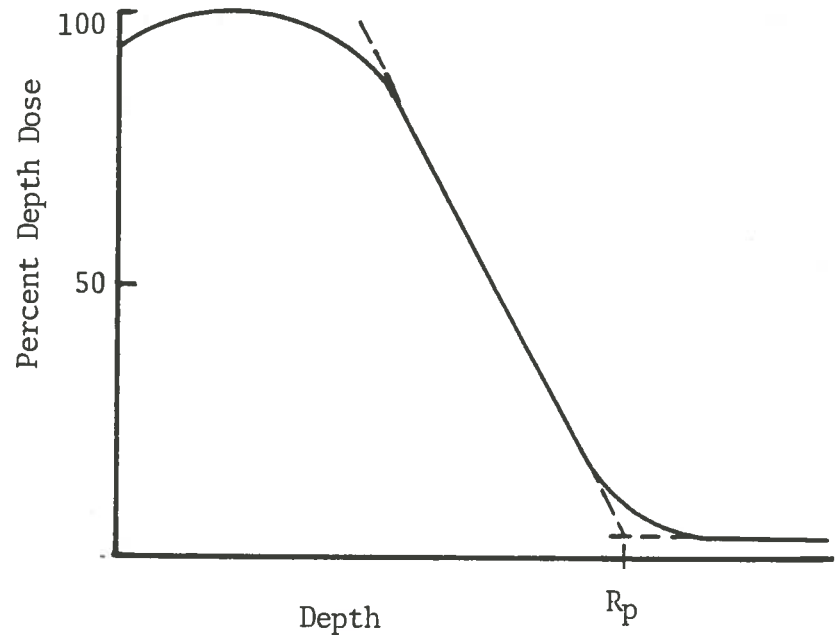

Figure 22. Depth-dose curve illustrating the definition of practical range (Khan, 1984).

Table 3

The Effect of Angular Errors on the Dose at d_{max}

For the Non-Beveled Cones

Energy (MeV)	Cone Diameter (cm)	Angular Error (degrees)	Decrease in R (%)(a)
9	3.0	2	2.3
9	3.0	3*	9.2
9	3.0	5	32.8
9	3.8	2	3.4
9	3.8	3*	10.3
9	3.8	5	31.2
9	4.3	2	NAC**
9	4.3	3*	5.3
9	4.3	5	23.3
9	5.0	2	1.8
9	5.0	3*	5.3
9	5.0	5	27.8
12	3.0	2	NAC
12	3.0	3*	4.7
12	3.0	5	34.3
12	3.8	2	NAC
12	3.8	3	NAC
12	3.8	5*	19.9
12	4.3	2	NAC
12	4.3	3	1.7
12	4.3	5*	17.1
12	5.0	2	1.3
12	5.0	3	3.6
12	5.0	5*	25.6
16	3.0	2	1.1
16	3.0	3*	5.7
16	3.0	5	39.6
16	3.8	2	NAC
16	3.8	3	NAC
16	3.8	5*	20.0
16	4.3	2	NAC
16	4.3	3	NAC
16	4.3	5*	14.6
16	5.0	2	NAC
16	5.0	3	1.9
16	5.0	5*	22.8

Table 3. The Effect of Angular Errors on the Dose at d_{max} (Continued)

Energy (MeV)	Cone Diameter (cm)	Angular Error (degrees)	Decrease in R (%)(a)
20	3.0	2	NAC
20	3.0	3*	5.2
20	3.0	5	41.6
20	3.8	2	NAC
20	3.8	3	1.5
20	3.8	5*	23.0
20	4.3	2	NAC
20	4.3	3	NAC
20	4.3	5*	14.1
20	5.0	2	NAC
20	5.0	3	1.1
20	5.0	5*	22.3

For the Beveled Cones (45°)

NOTE: Angular errors made in the plus and minus directions are indicated with "+" and "-" signs, respectively.

Energy (MeV)	Cone Diameter (cm)	Angular Error (degrees)	Decrease in R (%) (a)
9	3.0	+3	3.4
9	3.0	+4*	13.3
9	3.0	-1*	8.3
9	3.0	-2	17.9
9	5.0	+2	1.1
9	5.0	+3*	6.1
9	5.0	-1	1.6
9	5.0	-2*	5.3
12	3.0	+2	NAC
12	3.0	+3*	10.1
12	5.0	+3	NAC
12	5.0	+4*	5.0
16	3.0	+2	↑1.4***
16	3.0	+3*	4.8
16	5.0	+3	1.3
16	5.0	+4*	4.8

Table 3. The Effect of Angular Errors on the Dose at d_{max} (Continued)

Energy (MeV)	Cone Diameter (cm)	Angular Error (degrees)	Decrease in R (%)(a)
20	3.0	+2	NAC
20	3.0	+3*	5.5
20	3.0	-1	3.8
20	3.0	-2*	7.1
20	5.0	+3	NAC
20	5.0	+4*	4.6
20	5.0	-3	2.5
20	5.0	-4*	5.1

(a) R is the average of the 3 readings taken at each data point

* angular errors which first produced a significant decrease in the reading; all errors greater than these produced significant effects

** if the reading decreased by 1% or less, then it was considered as no apparent change (NAC)

*** The arrow indicates an increase in the reading rather than a decrease

energy. When the 9 MeV beam was used, the effect was much greater than that produced by the three higher energies. Even when the 3.8 cm cone (the next largest) was used with the 9 MeV beam, a 3° error continued to produce a significant effect. But as long as the energy was 12 MeV or greater and the cone employed was larger than 3.0 cm, no significant effect was seen with errors of 3° or less. Table 3 indicates that when 16 and 20 MeV beams were employed with the 3.0 cm flat-end cone, the effect of angular errors of 5° was greater than when the two lower energy beams were employed. Thus when the cone was too small the effects were magnified (instead of reduced) with the two higher energies. A 4° error was not investigated with the flat-end cones, but a 5° angular error produced large reductions in the dose at d_{max}, regardless of cone diameter or beam energy. However, it is highly unlikely that an error of this magnitude would occur, because it is such an obvious error.

Regarding the beveled cones, when the 12, 16, or 20 MeV beams were applied, greater effects were consistently produced when the smaller (3.0 cm) cone was employed. However, some inconsistencies were encountered when the 9 MeV beam was employed. For example, the 3.0 cm beveled cone, which was expected to produce a greater effect than the large cone, produced less effect when the errors were made in the "plus" direction using the 9 MeV beam. Table 3 shows that when the 9 MeV beam was employed with the smaller cone, a 3° error in the "plus" direction caused only a 4 percent decrease in the readings, while the same error applied with the larger cone caused a slightly higher (rather than lower), 6 percent decrease. But the expected results were seen with errors in the "minus" direction -- they produced greater effects when the

smaller cone was employed. In fact, when the 5.0 cm cone was employed, a 2° error ("minus" direction) produced less effect than a 1° error (also "minus" direction) when the 3.0 cm cone was used.

With respect to the flat-end cones (particularly the two smallest cones) there seemed to be no question in the data that the higher energies were less affected by the angular errors (except for the already specified 5° error); although the 16 and 20 MeV beams produced virtually the same results, and the 12 MeV beam differed only slightly, a substantially greater reduction in the readings was seen when the 9 MeV beam was utilized. Regarding the beveled cones, the 16 and 20 MeV beams again produced very similar results, with the 12 MeV beam differing somewhat (Table 3). But instead of seeing less effect with the 12 MeV than with the 9 MeV beam, when the 3.0 cm cone was used, a greater effect was seen. Note in Table 3 that a 3° error in the "plus" direction produced an 11 percent decrease in the average reading when the 12 MeV beam was used, compared to only a 4 percent decreased when the 9 MeV beam was used. But when the same two beams were applied with the larger cone, as expected, less of an effect was again produced by the higher energy.

When dealing with the beveled cones, errors as small as 1° and 2° made in the crucial direction, (the minus direction in this study) decreased the readings by as much as 9 or 10 percent if the cone was too small or the energy too low. For example, even when the energy was 20 MeV, if the cone was only 3.0 cm, a 9 percent decrease in the average reading was produced by a minus 2° angular error. Also note, when the larger cone was employed with the 20 MeV beam, a minus 4° error (rather than minus 2°) was required to produce a significant effect.

Because of the ease and reproducibility of the setup for the non-beveled cones, the setup was probably relatively free of errors, thus generating very consistent data. On the other hand, the setup for the beveled cones was more complicated, increasing the likelihood of setup errors. One might assume that setup errors were responsible for the inconsistencies pointed out earlier. However, the experiment involving the beveled cones should be redone in its entirety, in order to eliminate doubt and to assure the accuracy and reproducibility of a setup such as this.

Cone Ratios

In determining the cone ratios, at first a transvaginal cone (4.3 cm non-beveled cone) was used as the reference cone. The standard 10x10 cone was later used as the reference cone since it is employed to calibrate the linacs and therefore serves as a familiar reference point.

Initially cone ratios were determined with film in order to assure that the number of monitor units delivered would produce optical densities on the linear portion of the dose response curve. The cone ratios were later verified with an ion chamber and the data comparing both methods are presented in Table 4.

Regarding the non-beveled cones, the one with an inside diameter of 3.8 cm proved to have the highest output for each electron energy used. The smallest cone (3.0 cm) produced the lowest output for the 9 MeV beam while the largest cone (5.0 cm) produced the lowest output for the three higher energy beams.

With respect to the beveled cones, the smaller cone produced a higher output than the larger one, regardless of the electron energy.

Table 4

Cone Ratios Determined with Film and Ionization Chamber

E* (MeV)	Cone Diameter (cm)	Bevel (degrees)	C.R. Film[a]	C.R. from I.C.[b]	Difference (%)[c]	C.R. from I.C. (10x10)[d]
9	3.0	0	0.912	0.966	5.9	0.485
	3.8	0	1.049	1.074	2.4	0.539
	4.3	0	1.000	1.000	Ref. Cone	0.501
	5.0	0	0.941	0.945	0.4	0.474
12	3.0	0	1.000	1.007	0.7	0.581
	3.8	0	1.063	1.066	0.3	0.615
	4.3	0	1.000	1.000	Ref. Cone	0.576
	5.0	0	0.911	0.948	4.1	0.547
16	3.0	0	1.053	0.050	2.8	0.617
	3.8	0	1.080	1.070	1.0	0.629
	4.3	0	1.000	1.000	Ref. Cone	0.587
	5.0	0	0.920	0.966	5.0	0.567
20	3.0	0	1.050	1.048	0.2	0.613
	3.8	0	1.050	1.058	0.8	0.619
	4.3	0	1.000	1.000	Ref. Cone	0.585
	5.0	0	0.933	0.976	4.6	0.571
9	3.0	45	1.085	1.084	0.1	0.546
	5.0	45	1.075	1.073	0.2	0.540
12	3.0	45	1.086	1.055	2.9	0.612
	5.0	45	1.052	1.047	0.5	0.608
16	3.0	45	1.095	1.155	5.5	0.684
	5.0	45	1.071	1.065	0.6	0.631
20	3.0	45	1.123	1.170	4.2	0.684
	5.0	45	1.046	1.064	1.7	0.622

(a) cone ratios determined with film, normalized to the 4.3 cm 0° cone

(b) cone ratios determined with Modified Farmer-Type ionization chamber, normalized to the 4.3 cm 0° cone

(c) percent difference between results obtained with film and results obtained with ion chamber

(d) cone ratios determined with Modified Farmer-Type chamber, normalized to the conventional 10x10 cm applicator

(*) energy

Interestingly, both beveled cones produced higher outputs than any of the flat-end cones.

Although many feel that errors of at least 6 percent are inevitable when film is employed, the data in Table 4 support the notion that a strict quality assurance can eliminate the majority of errors as large as 6 percent.

Leakage

Leakage radiation is any radiation which strays from the useful portion of the beam (Khan, 1984). As previously described, the leakage was measured through film dosimetry. The net optical density readings obtained from the film were converted to dose using the sensitometric curves already presented. The leakage data measured at the air gap are presented in Table 5.

For 9 MeV electrons, the leakage measured at the air gap did not exceed 6 percent of the delivered dose, but rose to 11 percent for the 20 MeV beam. The leakage radiation for the 12 and 16 MeV beams fell between the measurements for the 9 and 20 MeV electrons. It is important to note that the optical density readings reported in Table 5 are the highest obtained from the film, and occurred in a very small area near the center of each piece of film. In addition, for reasons still undetermined, the leakage radiation at the air gap was highest at position No. 4 when the 16 and 20 MeV beams were applied (Figure 11).

Regarding the leakage radiation on the outer surface of each cone, measurements for the 5.0 cm cone were lower than for the 3.0 cm cone, especially when the 9 MeV beam was utilized. When 9 MeV electrons were applied with the 5.0 cm cone, the peak leakage was a mere 1 percent of

Table 5

Leakage Radiation Measured at the Air Gap[a]

Energy (MeV)	Position of Film	Highest Net O.D.[b] Readings	Leakage Radiation (%)[c]
9	No. 1	0.15	5
9	No. 2	0.16	6
9	No. 3	0.18	6
9	No. 4	0.18	6
12	No. 1	0.22	7
12	No. 2	0.24	8
12	No. 3	0.24	8
12	No. 4	0.24	8
16	No. 1	0.29	9
16	No. 2	0.26	8
16	No. 3	0.27	8
16	No. 4	0.33	10
20	No. 1	0.35	10
20	No. 2	0.31	10
20	No. 3	0.34	10
20	No. 4	0.39	11

(a) the non-beveled cone with an inside diameter of 5.0 cm was employed

(b) net optical density, i.e., base fog, has been subtracted

(c) the net optical densities were converted to dose using the sensitometric curves, and the leakage radiation is presented as a percentage of the delivered dose

the delivered dose. However, the 20 MeV beam produced leakage as great as 13 percent of the delivered dose when the larger cone was employed. With respect to the smaller cone, the highest measured leakage was 6 percent of the delivered dose for 9 MeV electrons, increasing to 15 percent for 20 MeV electrons.

When measuring leakage on the outer surface of the cones, the highest optical density readings were obtained at the top portion of each piece of film which was situated directly under the aluminum housing (Figure 11). The amount of leakage decreased consistently and significantly moving down the cone toward the phantom (Table 6).

The leakage measured is considered acceptable, since the cones are principally designed as transvaginal cones, which are primarily used to boost. The tumor dose delivered as a boost is not considered in the dose calculations; therefore the leakage is not, either. In addition, 20 MeV electrons are rarely used, but in case of their use, the energy of the leakage is relativley low. However, a supplementary shield could be employed when needed, rather than increasing the weight of a device that is sufficient for the majority of cases. Of course, with intraoral use, leakage is more significant. However, 20 MeV electrons are even more rarely used intraorally. Before any absolute data is reported, the leakage measurements obtained from film should be verified with an ion chamber.

Table 6

Leakage Radiation Measured on the Cone Surface

E (MeV)	Cone Diameter[a] (cm)	Position of O.D. Reading[b]	Leakage Radiation (%)[c]
9	3.0	highest	6
9	3.0	lowest	3
9	5.0	highest	<1
9	5.0	lowest	<1
12	3.0	highest	8
12	3.0	lowest	3
12	5.0	highest	5
12	5.0	lowest	1
16	3.0	highest	11
16	3.0	lowest	4
16	5.0	highest	8
16	5.0	lowest	2
20	3.0	highest	15
20	3.0	lowest	5
20	5.0	highest	13
20	5.0	lowest	3

(a) only non-beveled cones were employed

(b) optical density readings obtained directly under the aluminum housing are the highest while those readings obtained near the phantom surface at the base of the cone are the lowest

(c) the leakage radiation is presented as a percentage of the delivered dose

CONCLUSIONS AND RECOMMENDATIONS

Errors of 3° produced significant (5 percent or greater) reductions in the readings (with the chamber at d_{max}) when the 3.0 cm non-beveled cone was used, regardless of the energy of the beam, and when the 9 MeV beam was applied, regardless of the size of the cone. For the non-beveled cones larger than 3.0 cm, significant effects were not seen until errors of 5° were made, except when the 9 MeV beam was employed. Regarding the beveled cones, reductions in the readings at d_{max} also depended on the direction in which the errors were made. When the 3.0 cm beveled cone was employed with the 9 MeV beam, a 1° error in the "minus" direction produced significant effects while a 4° error in the "plus" direction was needed to do the same. A 2° error (minus direction) produced significant effects when the 9 MeV beam was applied with the larger beveled cone and when the 20 MeV beam was applied with the smaller beveled cone. In contrast, when the energy was 20 MeV and the larger cone was employed, errors less than 4° had no significant effects. When the 12 and 16 MeV beams were applied with the beveled cones, only errors in the "plus" direction were evaluted. For both energies, a 3° error produced significant effects when the smaller cone was used, while a 4° error did the same when the larger cone was employed.

The results of this study revealed that significant effects could be produced with angular setup errors as small as 1°, that is, when the 3.0 cm cone with a 45° bevel was employed, a 1° error in the minus direction caused the readings at d_{max} to decrease significantly. However, in the majority of the cases in this study, errors as great or greater than 3°

were necessary to significantly reduce the readings at d_{max}. Errors of this magnitude were obvious during setup while errors of 1 or 2 degrees were not. However, since this study excluded bevels greater and less than 45°, one might want to investigate additional cones before deciding to incorporate an expensive modification into the system. On the other hand, because of the care taken and the time involved in the setups of this study, it is the writer's opinion that the situation warrants an improved alignment system in order to assure quick and accurate alignment. One might consider incorporating a laser alignment system such as Seimens offers with their new non-docked intraoperative cone (Siemens Medical Systems, Inc., 1988) or a sophisticated camera system such as the one that Jones, et. al., described.

Certainly, the concept of a non-docked transvaginal cone system deserves to be pursued and perfected in order to decrease the risk of injury to the patient and to improve the quality of therapy.

BIBLIOGRAPHY

American Cancer Society (ACS). 1983. *Clinical Oncology for Medical Students and Physicians - A Multidisciplinary Approach*. American Cancer Society, New York, NY, pp. 4, 428-429, 458.

Biggs, P. J. and Wang, C. C. 1982. An intraoral cone for an 18 MeV linear accelerator. *International Journal of Radiation Oncology, Biology, and Physics*. Vol. 8, pp. 1251-1256.

Biggs, P. J. and Wang, C. C. 1984. Breakaway safety feature for an intraoral cone system. *International Journal of Radiation Oncology, Biology, and Physics*. Vol. 10, pp. 1117-1119.

Brichner, W. M. 1903. How to secure the best skiagrams; some practical points in the manipulation of vacuum tubes in radiography and radiotherapy. *International Journal of Surgery*, N.Y., Vol. 16, pp. 303-306.

Caldwell, E. W. 1902. New apparatus for therapeutic application of the roentgen ray to the larynx, tongue, rectum, prostate, cervix, etc. *New York Medical Journal*. Vol. 76, pp. 47-49.

Caulk, R. M. 1956. Review of seventeen years' experience with transvaginal roentgen therapy in cervical cancer. *Radiology*. Vol. 76, No. 5, pp. 965-969.

Del Regato, J. A. 1948. Role of transvaginal roentgen therapy in the treatment of carcinoma of the cervix. *Surgery, Gynecology, and Obstetrics*. Vol. 86, pp. 480-486.

Del Regato, J. A. and Cox, J. D. 1965. Transvaginal roentgen therapy in the conservative management of carcinoma in situ of the uterine cervix. *British Journal of Roentgentherapy*, Vol. 84, pp. 1090-1095.

Del Regato, J. A. and Ackerman, H. J. 1977. *Cancer Diagnosis, Treatment, and Prognosis*. The C. V. Mosby Company, St. Louis. pp. 785-786.

Dudley, R. A. 1956. Photographic film dosimetry. *Radiation Dosimetry*. G. J. Hine and G. L. Brownell, Eds. Academic Press, Inc. New York, NY.

Dutreix, J. and Dutreix, A. 1969. Film dosimetry of high energy electrons. *Annals*. N. Y. Academy of Science. 131, pp. 33-43.

Ehrlich, M. 1954. Photographic dosimetry of x and γ rays. *NBS Handbook 57*. Washington, DC.

Merrit, E. A. 1921. Possibilities of intravaginal x-ray therapy with description of the technique. *Journal of Radiology*. Vol. 2, pp. 29-34.

Merrit, E. A. 1937. A simple technique for intravaginal roentgen therapy. *American Journal of Roentgenology*. Vol. 37, No. 2, pp. 226-269.

Merrit, E. A. 1939. Roentgen therapy of cancer in the buccal cavity and of the cervix uteri. *American Journal of Roentgenology*. Vol. 42, No. 3, pp. 418-422.

Pennington, J. R. March, 1909. X-ray tube shields and specula for treating cancer of the rectum and other cavities. *The Philadelphia Medical Journal*. Vol. 10, No. 13, pp. 943-945.

Schneider, A. 1982. Radiation leakage from an electron applicator assembly on a linear accelerator. *Medical Physics*. Vol. 5, pp. 761-762.

Seimens Medical Systems, Inc. October, 1988. New intraoperative cone system. Presented at the *American Society for Therapeutic Radiology and Oncology*. New Orleans, LA.

Swindell, W. 1983. An endocavitary irradiator: two modifications for improved utility. *International Journal of Radiation Oncology, Biology, and Physics*. Vol. 9, pp. 111-112.

Tapley, N. duV. 1976. *Clinical Applications of the Electron Beam*. John Wiley & Sons. New York/London/Canada. pp. 25-26.

Wilson, D. L. Sharima, S. C., and Jose, B. 1986. An intracavitary cone system for electron beam therapy using a Therac 20 linear accelerator. *International Journal of Radiation Oncology, Biology, and Physics*. Vol. 12, pp. 1007-1011.

Wu, A., Kalend, A. M., and Sternick, E. S. Nov./Dec. 1984. Comments on the method of energy determination for electron beams in the TG-21 protocol. *Medical Physics*, Vol. 11, No. 6, pp. 871-874.

VITA

Mary Jeanne Haik was born on April 1, 1958 in Covington, Louisiana. She attended Covington High in Covington and graduated with honors in May 1976. In December 1982 she graduated from Louisiana State University in the top 6% of her class with a Bachelor of Science degree in Psychology. She began her post-graduate work in August of 1986 when she entered graduate school in Nuclear Science at Louisiana State University. In January 1987 she recieved a full graduate assistantship which was transferred to the Clinical Physics Department of Mary Bird Perkins Cancer Center in August 1987. She is currrently a candidate for the Master of Science Degree in Nuclear Science, Medical Radiation Science Option.